New evidence for syntectonic fluid migration across the hinterland-foreland transition of the Canadian Cordillera

Stuart R. Knoop, Lori A. Kennedy, and Gregory M. Dipple

Department of Earth and Ocean Science, University of British Columbia, Vancouver, British Columbia, Canada

Received 19 September 2000; revised 21 September 2001; accepted 2 October 2001; published 17 April 2002.

[1] Oxygen isotope data from syntectonic veins, thrust faults, and wall rocks suggest that fluids infiltrated the Western Ranges of the Rocky Mountain foreland from deeper rocks of the Dogtooth Range during Mesozoic contraction. This signifies the first such evidence for kilometer-scale fluid migration at the hinterland-foreland transition of the Canadian Cordillera. Fluid infiltration resulted in isotopic depletion in wall rocks and isotopic disequilibrium between veins (fluid) and their host rocks downstream of a lithologic, structural, and isotopic shift between predominantly siliciclastic (Dogtooth Range) and calcareous (Western Ranges) sequences. The shift corresponds with an average $\delta^{18}O$ that is 3.0‰ higher in the Western Ranges. In the Dogtooth Range, atypically low carbonate values (15.6‰ ± 0.8‰ (VSMOW)), and the consistency with which vein signatures approach the average bulk rock $\delta^{18}O$ of individual outcrops indicate fluid buffering by a siliciclastic reservoir and outcrop-scale (10–100 m) fluid circulation. In contrast, rocks and veins in the Western Ranges exhibit a gradational increase in $\delta^{18}O$ that extends $\geq$14 km eastward and up section from the isotopic shift and possess values that are below or at the low end of typical carbonate compositions (16.2–20.9‰ (VSMOW)). Furthermore, veins systematically exhibit lower oxygen values than their host rocks; this implies that the fluids that entered the Western Ranges were in modest disequilibrium with the rocks through which they flowed. We use a one-dimensional reactive transport model to infer that rocks in the Western Ranges experienced a time-integrated fluid flux of 1.1×10^5 mol H_2O cm^{-2} ($\approx 2.4 \times 10^6$ cm^3 cm^{-2}) and sluggish reaction kinetics during the flow event. *INDEX TERMS:* 8102 Tectonophysics: Continental contractional orogenic belts; 8010 Structural Geology: Fractures and faults; 8045 Structural Geology: Role of fluids; 1045 Geochemistry: Low-temperature geochemistry; *KEYWORDS:* Fluid flow, fluid-rock interaction, thrust fault, oxygen isotopes, Canadian Cordillera, hydrodynamic dispersion

1. Introduction

[2] Syntectonic fluid migration can influence the mechanical, petrological, and geochemical properties of rocks along a flow path. Numerous studies have explored the potential for large-scale fluid flow during orogenesis and metamorphism (as reviewed by *Oliver* [1996]) and its role in the generation of geochemical fronts [*Bradbury and Woodwell*, 1987; *Ferry*, 1992], mineral deposits [*Oliver*, 1986], and hydrocarbon reservoirs [*Oliver*, 1986; *Machel et al.*, 1996]. This paper provides the first evidence of kilometer-scale, syncontractional fluid infiltration into the foreland of the western Canadian Rockies. In addition, it records the first use of robust structural data to constrain the relative timing of a regional fluid flow event in this portion of the Cordillera. Our analysis focuses on a structurally and lithologically defined oxygen isotopic boundary, across which we can detect the subtle effects of fluid migration and isotopic alteration of host rocks. By sampling pairs of syntectonic veins and wall rocks we also document patterns of fluid-rock isotopic disequilibrium, which is incorporated into a reactive transport model that provides reasonable estimates for time-integrated fluid flux and kinetic dispersion.

[3] In past studies, researchers have cited systematic oxygen isotope depletions and large changes in major element concentration within both basement and supracrustal shear zones to justify deep (upper greenschist to granulite facies) and voluminous ($\cong 10^4$–10^5 m^3 m^{-2}) infiltration of meteoric and metamorphic fluids during contraction [e.g., *Burkhard and Kerrich*, 1988; *Marquer and Burkhard*, 1992; *Dipple and Ferry*, 1992a; *Cartwright and Buick*, 1999]. For example, *Marquer and Burkhard* [1992] interpreted isotope depletions in shallow level (200°–300°C), carbonate hosted late stage veins and mylonites in the Swiss Alps as evidence that kilometer-scale interconnectivity between shear zones promoted fluid expulsion upward from crystalline basement. In contrast, other case studies infer that regional deformation by pressure solution and faulting need not be accompanied by extreme volume loss or a large time-integrated fluid flux [e.g., *Gray et al.*, 1991; *Cartwright et al.*, 1994; *Kirschner and Kennedy*, 2001]. On the basis of low isotopic variation between fault rocks and their adjacent protolith, *Kirschner and Kennedy* [2001] found no evidence for extensive fluid advection outside of very narrow shear zones in the Front Ranges of the Canadian Rockies. In a dramatic example from the Lachlan fold belt of southeastern Australia, *Gray et al.* [1991] demonstrated that diffusion and advection over relatively short distances (tens to hundreds of meters) combined to promote the isotopic homogenization of quartz veins in thrust sheets and faults across 80,000 km^2.

[4] *Nesbitt and Muehlenbachs* [1994, 1995, 1997] used data from fluid inclusions and hydrogen and oxygen isotopes to assert that fluid flow during Mesozoic contraction was minimal in the Purcell and western Rocky Mountains (including our study area).

0148-0227/02/2001JB000217$09.00

They argued that most veins record either a pretectonic phase of fluid flow related to early metamorphism or result from the channeling of meteoric waters downdip along normal faults during Early Tertiary extension. This paper expands upon previous work and provides an alternative interpretation of substantial syntectonic fluid migration. Specifically, our contribution (1) documents an isotopic shift and explores in detail the implications of this structurally and lithologically defined boundary, (2) places explicit constraints on the relative timing of veins and fault-related fabrics and links them with geochemical data, and (3) provides extensive analysis and discussion of the isotopic composition of lithologically diverse wall rocks.

[5] This study utilizes oxygen isotopes from more than 100 samples of wall rock, synkinematic veins, and fault breccia to interpret both outcrop-scale (<500 m) and regional (>1 km) fluid regimes. The sampling transect extends 30 km across strike from the Dogtooth Range in the northern Purcell Mountains, across the Rocky Mountain Trench (RMT), and into the Western Ranges of the Rocky Mountain foreland (Figures 1 and 2). The Purcell Thrust, an out of sequence fault that separates predominantly siliciclastic sedimentary rocks of the Dogtooth Range from younger, calcite-dominated sequences in the RMT and Western Ranges loosely coincides with the hinterland-foreland transition in the southern Canadian Cordillera. Importantly, it delineates an abrupt, regionally significant structural, stratigraphic, and isotopic boundary, where transport theory dictates that alteration from fluid migration will be most conspicuous [e.g., *Bickle and McKenzie*, 1987]. In light of difficulties presented in similar studies of the Front Ranges in the Canadian Rockies [*Woodwell*, 1985; *Kirschner and Kennedy*, 2001] where homogeneous carbonate reservoirs can easily diminish the isotopic imprint of throughgoing fluids, this provides an excellent opportunity to test for kilometer-scale fluid migration in the form of a migrating isotopic alteration front downstream of the Purcell Thrust.

2. Regional Overview

[6] The study area encompasses 1100 km^2 in southeastern British Columbia from the western Dogtooth Range near Glacier National Park to the central Western Ranges east of Golden, British Columbia. Since Late Proterozoic time, at least two phases of extension (Late Proterozoic-Early Cambrian and early Tertiary) and two compressional events (Devonian and Late Jurassic-Early Cretaceous) have been documented in the eastern Cordillera. Furthermore, a large-scale fluid event in pre-Jurassic time resulted in the dolomitization of Cambrian platform carbonates directly east of the study area [*Nesbitt and Muehlenbachs*, 1994; *Yao and Demicco*, 1995, 1997].

[7] The sampling transect straddles a major tectonic boundary between two morphogeological belts of the Canadian Cordillera (Figure 1). The Dogtooth Range occupies the eastern extent of the Omineca Belt, a province that contains the suture of marine sediments from the Upper Proterozoic and Lower Cambrian North American rift margin with accreted island arcs and oceanic crust of Late Paleozoic to Early Mesozoic age. The Western Ranges form the western boundary of the Foreland Belt, which is characterized by its thin-skinned style of deformation with broad, regional folds that overlie shallow-dipping decollements. Together, the Dogtooth and Western Ranges represent a structural transition from the polydeformed, greenschist to amphibolite grade rocks that comprise the Selkirk Complex in the west to the fault-dominated, foreland-type tectonism that affects subgreenschist assemblages in the platform carbonates of the Rocky Mountain Main and Front Ranges [*Gabrielse and Yorath*, 1992].

[8] Important to this study and the interpretation of stable isotope data, the two domains exhibit contrasting rock types. Turbiditic and coarser-grained shore face metasedimentary rocks of Proterozoic to Early Cambrian age dominate the Dogtooth Range [*Simony and Wind*, 1970; *Kubli*, 1990]. The Western Ranges host upper Cambrian to upper Ordovician shallow marine units assigned to the Canyon Creek Formation, McKay Group, and Beaverfoot Formation [*Balkwill*, 1972; *Gardner et al.*, 1976] (Figures 2 and 3). Consequently, wall rock composition varies substantially between the Dogtooth Range, where slate, phyllite, and sandstone possess <20 vol % carbonate minerals, and the Western Ranges, which comprise phyllite, limestone, and dolostone with >50 vol % calcite and dolomite.

3. Deformation

[9] The evolution of the Dogtooth Duplex, located at the northern terminus of the northwest trending Purcell Anticlinorium, resulted in ~18–23 km or 50% shortening. *Kubli and Simony* [1994] propose that the region evolved as a hinterland-dipping duplex during a main phase of contraction (D1) between late Jurassic and early Cretaceous time. Its deformation history is relatively simple and consists of a prolonged phase of northeast directed imbricate thrust faulting and associated regional folding with locally intense ductile shear [*Kubli and Simony*, 1994]. During D1 deformation, out-of-sequence displacement on major faults, such as the Quartz Creek Thrust in the central duplex, resulted in the tightening and overturning of structures in the west. Regional detachments that were examined in this study include, from west to east, the Heather Mountain, Quartz Creek, Cirque Creek, and Wiseman Creek Thrusts (Figure 2).

[10] During the interval between D1 and the development of a secondary foliation that formed during a transtensional phase, more than 10 km of displacement on the out-of-sequence Purcell Thrust led to the offset of faults and fabrics in the eastern Dogtooth Duplex and their juxtaposition against Upper Cambrian units of the Western Ranges [*Simony and Wind*, 1970; *Kubli and Simony*, 1994]. Approximately 3800 m of Middle Cambrian pelites from the Chancellor Formation, which separate units from the Dogtooth and Western Ranges, have been truncated by the Purcell Thrust and are therefore unexposed in this portion of the study area (Figure 2) [*Balkwill*, 1972; *Gardner*, 1977].

[11] The style of deformation in the Western Ranges reflects the incompetent rheology of the units that comprise them. Bulk strain has resulted in 30 km of shortening [*Kubli and Simony*, 1994] and is partitioned mainly into cleavage formed during pressure solution of quartz and calcite and recrystallization of muscovite and chlorite. Pervasive isoclinal folding and minor displacement (<3 km) on regional thrust faults occurred in conjunction with the development of axial planar cleavage [*Cook*, 1975].

[12] The Western Ranges' western margin coincides with the Rocky Mountain Trench, a northwest trending, topographically defined lineament that formed in Tertiary time and extends more than 1600 km [*van der Velden and Cook*, 1996]. Although dextral strike-slip displacement associated with the trench exceeds 400 km in the northern Cordillera, only minor transform and extensional faulting occurred in the southern Rockies. Importantly, major structures have been correlated directly across the trench near the latitude of this study on the basis of seismic reflection data [*van der Velden and Cook*, 1996], and therefore minimal strike-slip faulting does not restrict conclusions about syntectonic fluid communication between the Dogtooth and Western Ranges.

4. Metamorphism and P-T Conditions

[13] In the Dogtooth Range, pervasive chlorite and siderite record lower greenschist facies metamorphism, and *Kubli* [1990] used structural restorations to constrain the minimum depth of burial as 10 km at 3 kbar. On the basis of calcite-dolomite solvus thermometry in wall rocks, *Kubli* [1990] deduced a maximum burial temperature of 360–375°C. *Gardner* [1977] used phase equilibria and calcite-dolomite solvus thermometry to estimate

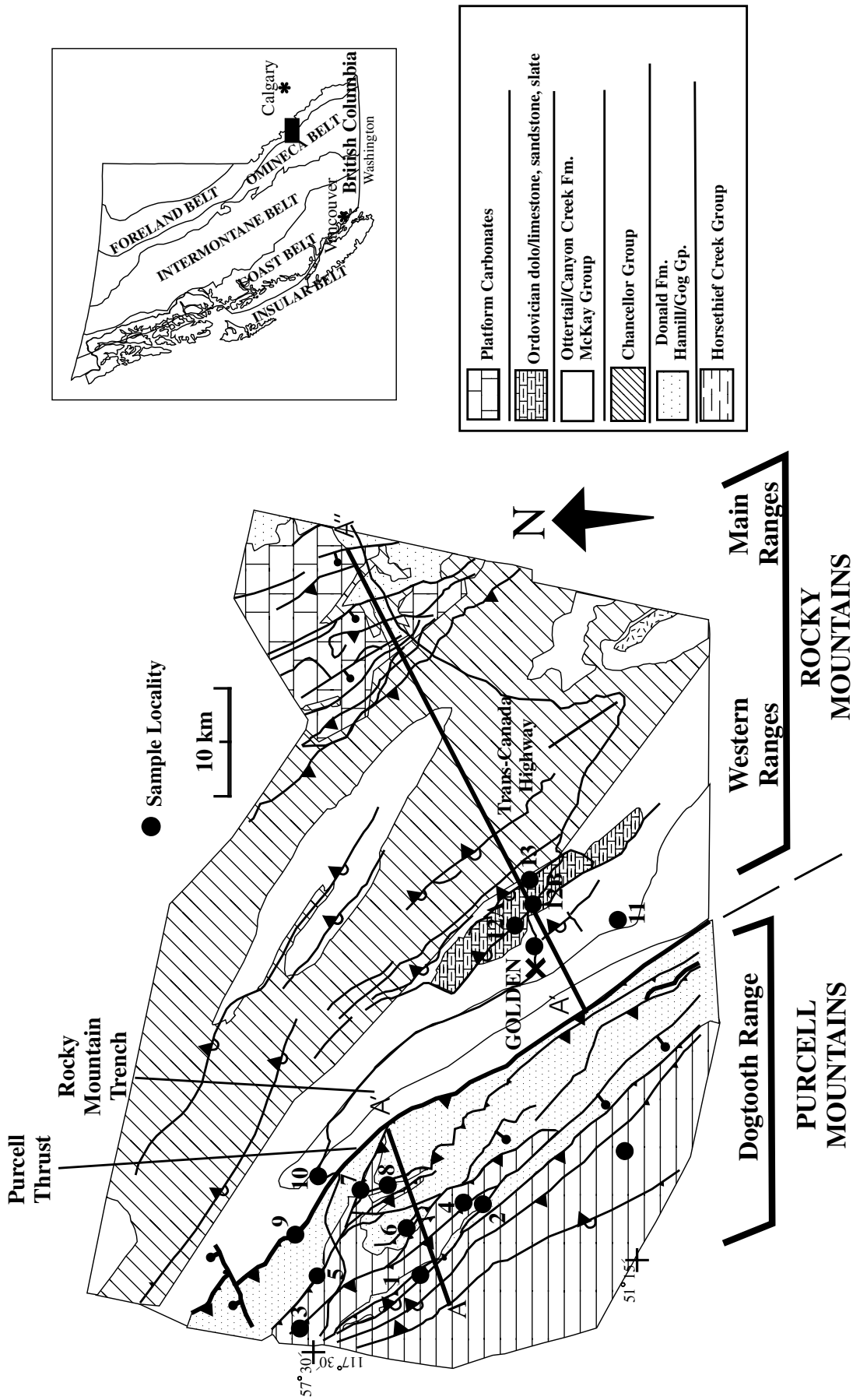

Figure 1. Regional map of study area including sample locations denoted by solid circles. Modified from *Price and Simony* [1971]. Cross section A-A″ is shown in Figure 2. Numbers correspond to localities listed in Tables A1 and A2.

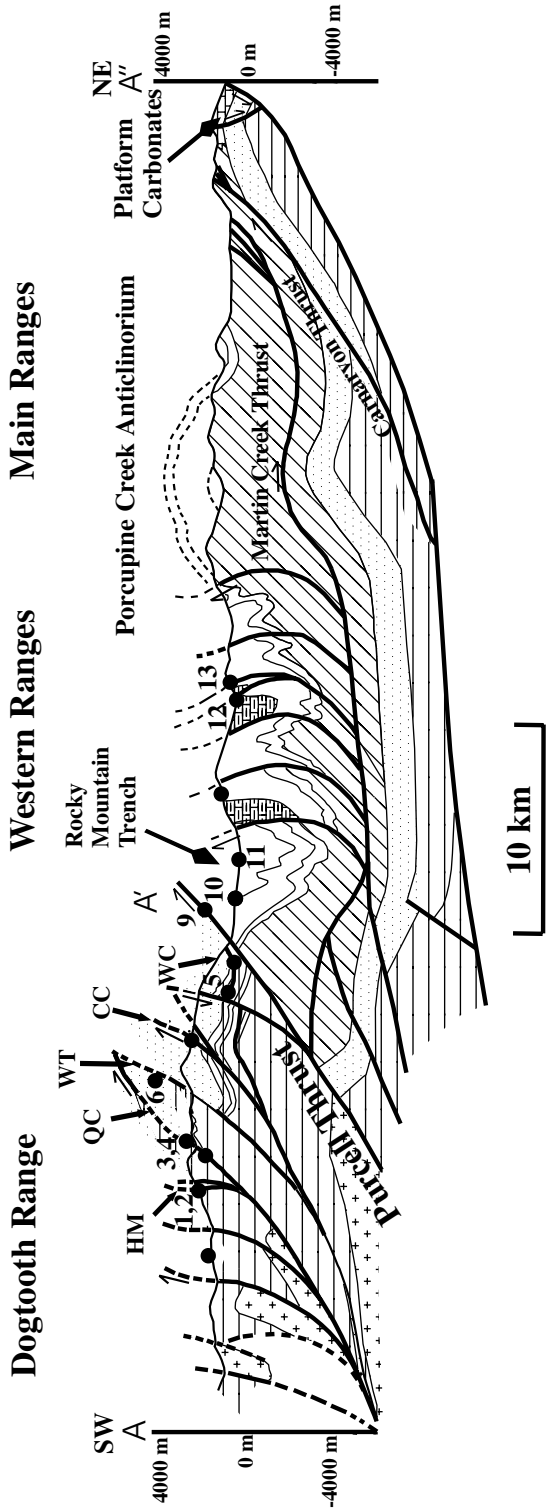

Figure 2. Simplified cross section of study area (location shown in Figure 1). Solid circles denote sample localities listed in Tables A1 and A2. Circles above topography reflect localities away from line of section. Modified from *Kubli* [1990], *Kubli and Simony* [1994], *Price and Simony* [1971], *Balkwill* [1969], and *Cook* [1970]. HM, Heather Mountain Thrust; QC, Quartz Creek Thrust; WT, Wall Thrust; CC, Cirque Creek Thrust; WC, Wiseman Creek Thrust.

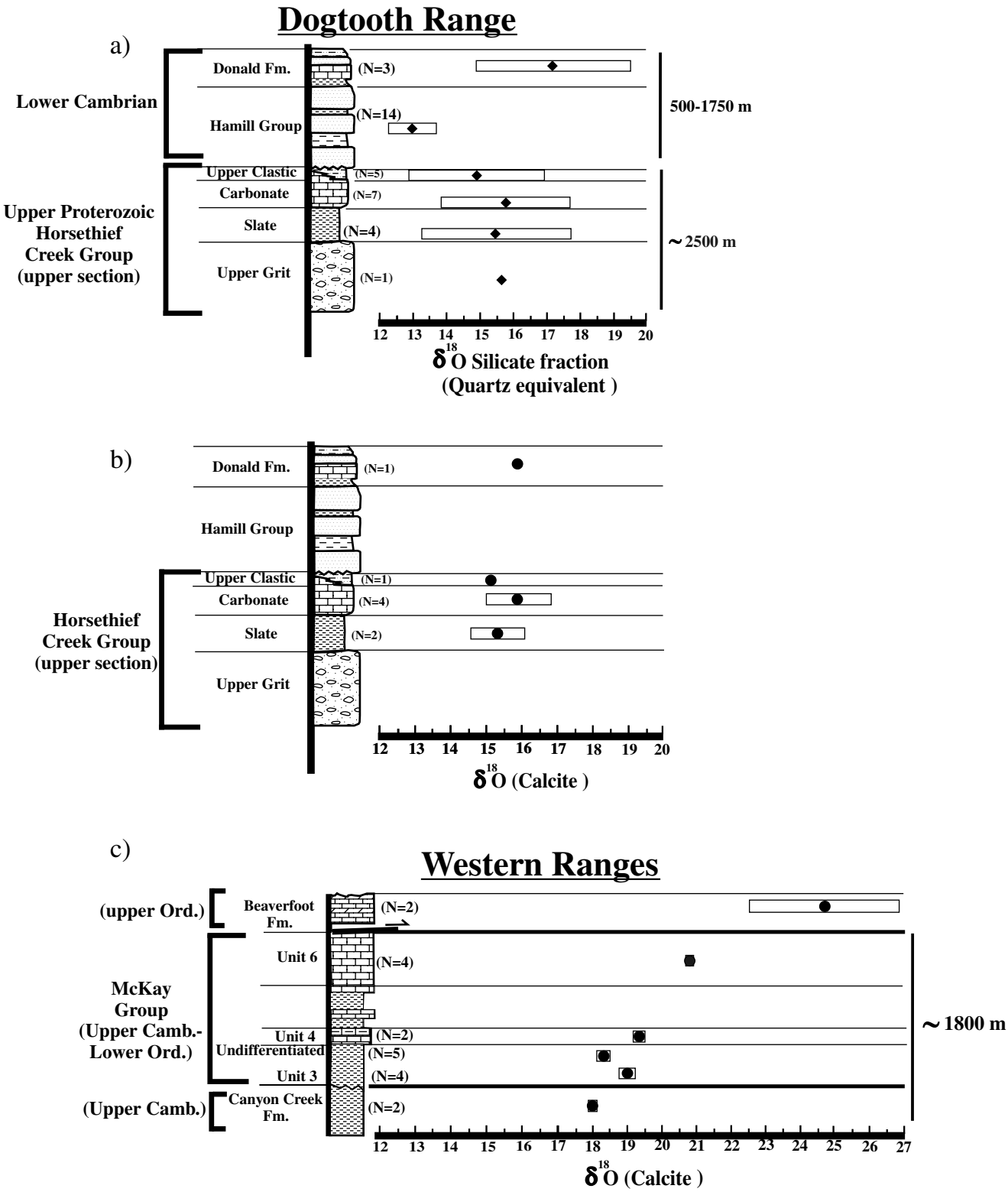

Figure 3. Distribution of oxygen isotope values by stratigraphic horizon. Bars denote 1σ of population. (a) and (b) Units from Dogtooth Range exhibiting no isotopic trend with decreasing age. Stratigraphic section modified from *Kubli and Simony* [1992]. (c) Units in the Western Ranges showing isotopic enrichment in younger units. Section modified from *Cook* [1975].

maximum P-T conditions that were consistent with chlorite grade metamorphism in the Western Ranges, with temperatures no greater than 365–420°C and pressures of at least 2.5 kbar. The exact timing of metamorphism with respect to deformation in the Dogtooth and Western Ranges is ambiguous. However, inclusion trails within siderite porphyroblasts from the Dogtooth Range demonstrate that peak metamorphism in the west occurred either during, or shortly after D1 deformation [*Kubli*, 1990]. Given that

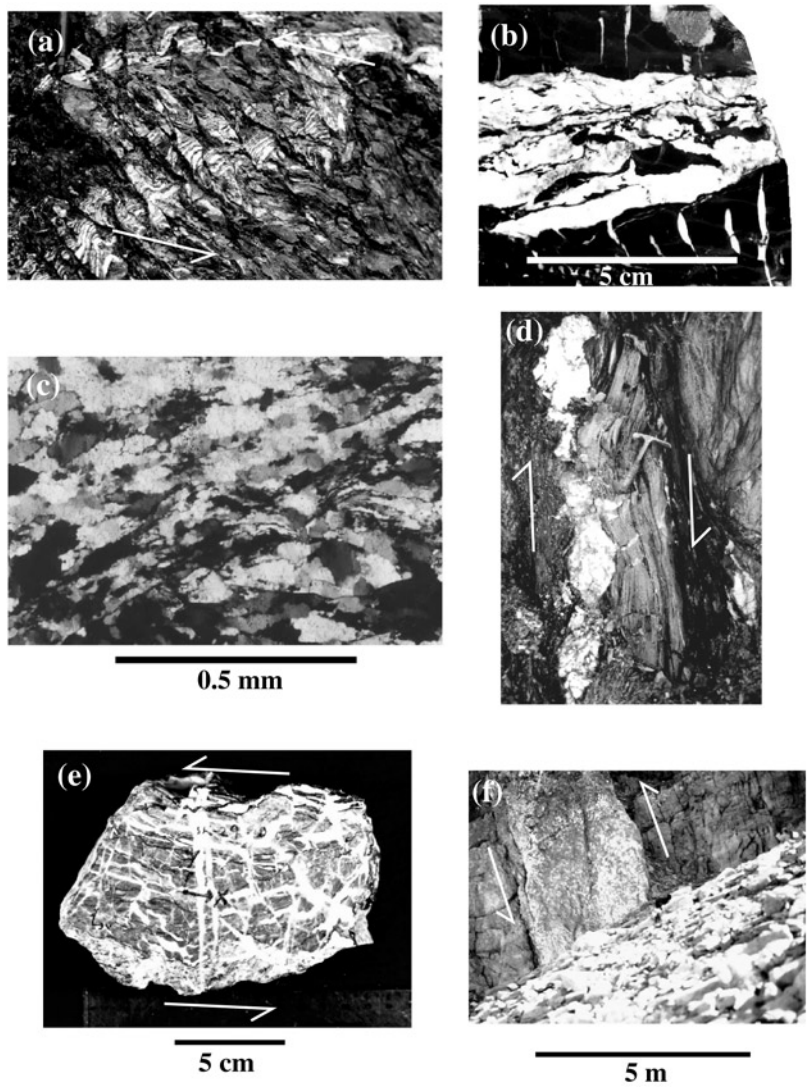

Figure 4. Representative veins from the Dogtooth and Western Ranges. Arrows indicate shear sense on vein. (a) Laminated, bedding parallel quartz-calcite veins near the Purcell Thrust. Note pen for scale. Sense of shear is top to the northeast. (b) Bedding-parallel vein with calcite-filled tension gashes oriented perpendicular to bedding. (c) Photomicrograph (x polar) showing incipient S fabric within a distended, cleavage-parallel quartz vein near the Quartz Creek Thrust (shown in Figure 4d). (d) Distended, cleavage-parallel vein near footwall splay of Quartz Creek Thrust. Sense of shear is top to the southwest. (e) Cataclasite from unnamed fault in the Western Ranges. Veins and stylolites are oriented oblique and parallel to the regional fabric. Sense of shear is top to the southwest. (f) Type 3 quartz vein at Cirque-Creek Thrust. Sense of shear is top to the northeast.

the main phase of deformation was likely synchronous in the Dogtooth and Western Ranges [*Kubli and Simony*, 1994], it is a reasonable assumption that metamorphism and associated devolatization reactions were broadly coeval with D1 and vein development throughout the study area. The pervasiveness of penetrative cleavage in the Western Ranges and evidence that deformation initiated when sediments were at their maximum depth of burial provide further support for syntectonic metamorphism.

5. Methodology for Sample Selection

[14] Because the scope of this study is limited to fluid regimes that evolved with structures during Mesozoic contraction, constraints on the timing of veining events were essential. In this paper, the term ''synkinematic'' will therefore denote events concurrent with the main phase of northeast directed, Mesozoic compression. Sampling localities have been chosen to highlight patterns of isotopic disequilibrium across the structural contact between the Dogtooth and Western Ranges, across individual faults, and within dense fracture zones of thrust sheets. Two types of settings are emphasized: (1) outcrops where regional thrust faults are exposed, including the Purcell Thrust, five faults in the Dogtooth Range, and two thrusts in the Western Ranges, and (2) exposures within thrust sheets where vein density is high (>10%), and crosscutting relationships between axial planar cleavage, minor faults, and veins permit robust timing constraints to be placed upon fluid events.

6. Geometry and Timing of Veins

[15] The style and prevalence of veining across the transect is heavily contingent upon the competence of host rocks and the mechanisms by which they deform. In the Dogtooth Range, veins are more prominent in coarse-grained, brittle units such as quartz-

Table 1. The $\delta^{18}O$ Compositions in the Dogtooth and Western Ranges[a]

	Mean $\delta^{18}O$	Mean $\delta^{18}O$ (qtz Equivalent)	Range	*n*
		Dogtooth Range: Horsethief Creek Group		
Siliciclastics	12.7 ± 2.1	15.1 ± 1.8	13.4–19.9 (qtz)	18
Carbonates	15.6 ± 0.8		14.7–17.3	7
Vein calcite	15.4 ± 1.4		13.8–16.3	4
Vein quartz	16.4 ± 2.2		14.5–19.7	8
		Dogtooth Range: Hamill Group and Donald Formation		
Siliciclastics	12.8 ± 1.4	13.8 ± 1.9	11.5–19.8 (qtz)	18
Carbonates	15.9			1
Vein calcite	16.2 ± 0.1		16.2–16.3	3
Vein quartz	14.6 ± 2.5		12.5–18.8	11
		Western Ranges: Canyon Creek Formation and McKay Group		
Siliciclastics	15.7	17.4		1
Carbonates	19.2 ± 1.1		17.9–20.9	14
Vein calcite/breccia	18.1 ± 1.1		16.2–20.0	20
Vein quartz	19.9 ± 1.6		18–22.3	6

[a] Uncertainty represented as 1σ of population; qtz, quartz equivalent.

ite, massive lime/dolostone, and siltstone, whereas in the Western Ranges they are equally distributed throughout slate, micrite, and siltstone. Macroscopic veining within Proterozoic slate and phyllite from the Dogtooth Range is sparse compared with similar lithologies in the Western Ranges, which commonly host dense fracture networks that record multiple fluid events.

[16] Vein density correlates with increased proximity to about half the regional faults studied, and veins are more common in outcrops that host minor splays and faults than outcrops with no faulting. Quartz- and carbonate-bearing veins were observed on both sides of the Purcell Thrust. Consistent with the composition of surrounding host rocks, quartz comprises most veins in the Dogtooth Range, whereas calcite and dolomite are the dominant vein constituents in the Western Ranges. Accessory vein-filling minerals include chlorite, muscovite, apatite, and pyrite. On the basis of their crosscutting relationship with S1 cleavage (which, unless crosscutting relationships are available, we infer to be related to Mesozoic contraction), folds, and faults, we categorize veins as early to syntectonic, syntectonic, and late tectonic (Figure 4). For a more detailed description of vein geometry and texture, see *Knoop* [2000].

[17] Early to syntectonic (type 1) veins include type 1a, kinked and sigmoidal veins oriented oblique to bedding and cleavage; type 1b, syntaxial, calcite-filled tension gashes oriented perpendicular to bedding; and type 1c, laminated to massive, bedding-parallel veins. Type 1a veins are 1- to 5-cm-wide and occur within broadly folded beds of quartzite and siltstone. Intragranular strain manifested as subgrain rotation and deformation lamellae and elongated, recrystallized grains oriented parallel to local cleavage indicate early tectonic development. Type 1b veins between 30 μm and 3 mm wide are usually vertical and commonly occur near the hinges of centimeter-scale folds, which suggests that they either precipitated while bedding was horizontal or formed later during extension perpendicular to fold axes (Figure 4b). These are crosscut by 2–6 cm wide, type 1c veins that form northwest trending, open to isoclinal, often rootless folds (Figures 4a and 4b). Successive generations of fibrous calcite, euhedral quartz and calcite, and very fine grained, disseminated apatite record a prolonged history of fluid infiltration by crack-seal and open fracture-filling mechanisms.

[18] Syntectonic (type 2) veins are variably distended, parallel to cleavage, and occur within slate and phyllite throughout the transect (Figures 4c and 4d). The absence of fold closure within type 2 veins and the fact that local bedding is not transposed into parallelism with cleavage indicate that they did not precipitate prior to cleavage development. Veins are not limited to outcrops where cleavage is vertical, as would be expected if they originated as mode I style tensile cracks perpendicular to bedding. Moreover, boudinage, which records subsequent flattening or elongation in the plane of cleavage (i.e., the *XY* plane), suggests that they do not postdate cleavage. Near the Quartz Creek Thrust in the Dogtooth Range, intense dynamic recrystallization of elongate quartz grains parallel to foliation and the growth of an incipient S-C shear fabric demand that veins formed prior to the cessation of contraction (Figure 4c). In the Western Ranges, cleavage-parallel veins are more pervasive and exhibit milder intragranular strain compared with those in the Dogtooth Range.

[19] Late tectonic (type 3) veins formed parallel to faults. These include densely fractured and stylolitized breccia zones that crosscut all other vein types and document the youngest phase of contraction-related fluid infiltration in the study area (Figures 4e and 4f). At each locality, thrust-parallel veins are often discontinuous along strike, indicative of variability in pressure gradients and fluid channeling into and along faults. Type 3 veins in the Dogtooth Range exhibit widths of up to 3 m and display a penetrative fabric defined by parallel, discontinuous muscovite seams. Quartz grains within microlithons possess a well-defined crystallographic preferred orientation and aspect ratios greater than 10:1.

[20] In the Western Ranges, fault contacts are bounded by a resistant, ~50-cm-wide "damage zone" of stylolites, millimeter-wide calcite veins, and calcite-dolomite matrix that has been both brecciated and dynamically recrystallized (Figure 4e). Matrix calcite has undergone intense grain size reduction from a diameter of 0.4 mm to <10 μm and exhibits a strong shape-preferred orientation parallel to the regional foliation. Laminated and massive veins between 5 and 10 cm in width also precipitate along meter-scale reverse faults at outcrops east of the Purcell Thrust.

7. Stable Isotope Analysis

[21] Results are based on 124 $\delta^{18}O$ analyses that were divided evenly between carbonates and silicates. Intralaboratory and interlaboratory comparisons between University of British Columbia (UBC) and Queen's University geochemistry laboratories were based upon submission of duplicate samples that yielded an analytical uncertainty of 0.1‰. In the following sections, the suffix "qtz equivalent" refers to oxygen values from polyphase silicates that have been normalized to quartz based upon estimates of

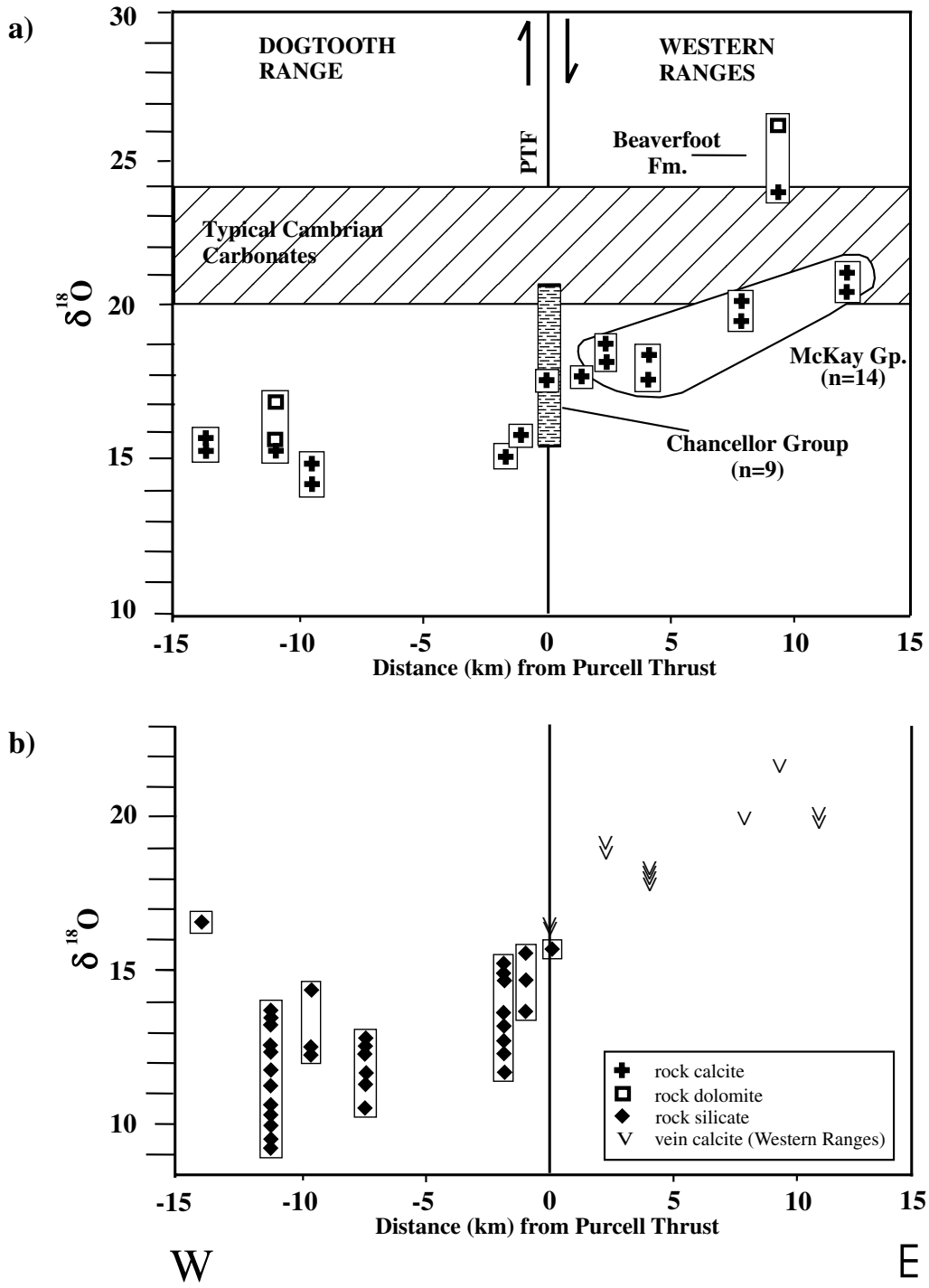

Figure 5. Oxygen isotope value of wall rock carbonates and silicates. Although 24 veins were sampled in the Western Ranges, not all are shown because of overlap among values. PTF, Purcell Thrust Fault. *X* axis is measured as distance across strike. The signature of carbonates from the Chancellor Group reflects the composition of Middle Chancellor units below the Upper Cambrian succession. Samples from the Chancellor Group were obtained 40 km east of the PTF in the Main Ranges [*Knoop*, 2000].

mineral mode and a quartz-mineral fractionation factor. A complete discussion of analytical techniques and associated uncertainties is provided in Appendix A.

7.1. Regional Distribution of $\delta^{18}O$ in Wall Rocks

[22] In this section we highlight critical differences in the distribution of wall rock compositions both within the Dogtooth and Western Ranges and across the structural contact that divides them. Mean oxygen values are presented in Table 1, and a complete listing of isotopic results are presented in Appendix A. Figures 5a and 5b convey (1) a sharp eastward increase in $\delta^{18}O$ (calcite) across the Purcell Thrust, (2) fairly constant $\delta^{18}O$ (calcite and quartz) values from sandstones and pelites both laterally and up section within the Dogtooth Duplex, and (3) a trend of gradual, eastward enrichment in $\delta^{18}O$ (calcite) up strati-

Table 2. Summary of Catalysts for Isotopic Depletion in the Western Ranges

Scenario	Conclusion	Evidence[a]
Shift in $\delta^{18}O$ is a function of age variability (closed-system)	no	observed isotopic spread is too large
Exchange with locally derived, metamorphic fluids (closed system)	partially responsible for outcrop-scale homogenization	correlation between $\delta^{18}O$ and silicate abundance in some outcrops but no correlation between phyllosilicate concentration and magnitude of depletions
Exchange with low-$\delta^{18}O$ phases (closed system)	partially responsible	evidence from McKay-Canyon Creek contact and correlation between $\delta^{18}O$ and silicate abundance in some outcrops
Fluid-rock thermal disequlibrium (closed- or open-system)	no	unrealistic given required temperature differen tial/vein geothermometry precludes this
Up temperature fluid flow (open system)	no	quartz veins preclude up temperature flow and required TIFFis too large
Exchange with low-$\delta^{18}O$, exotically derived fluid (open system)	yes	likely source reservoir in the Dogtooth Range and similarity between observed isotopic profile and model-derived profiles for regional fluid migration

[a] TIFF, time-integrated fluid flux.

graphic section and laterally across structural contacts in the Western Ranges.

[23] Compared with carbonates in the Dogtooth Range that exhibit a mean $\delta^{18}O$ (calcite) of 15.6 ± 0.8‰, those in the Western Ranges are consistently heavier in ^{18}O by 4.5‰, with an average of 20.1 ± 2.3‰. We observed no compositional overlap between the two domains, with the highest signature in the Dogtooth Range, 17.3‰, recorded in a 10-m-thick dolomite unit. By comparison, calcareous slate from the immediate footwall of the Purcell Thrust possessed a $\delta^{18}O$ of 17.9‰, the lowest in the Western Ranges. At the Purcell Thrust, where the eastern and western domains are directly juxtaposed, this shift is recorded in calcite from footwall slates that are enriched by 2.0‰ relative to carbonates ~150 m away in the hanging wall. Only one silicate analysis was obtained from wall rocks in the Western Ranges, where a phyllite from the Rocky Mountain Trench possessed a $\delta^{18}O$ (qtz equivalent) of 17.4‰. Comparatively, pelites in the Dogtooth Range are depleted by 1.2‰ and therefore record a similar, albeit less constrained, trend of lower values as that observed in carbonates.

[24] Siliciclastic rocks from the Horsethief Creek Group in the Dogtooth Range exhibit, on average, a relatively constant range of compositions regardless of their stratigraphic position or the thrust sheet in which they occur (Figure 3a). This suggests that differences in age, mineralogy, and sedimentary provenance between units leave no systematic imprint on their isotopic signature, or their effect has been overprinted by secondary processes. However, large standard deviations (~2.2‰) and a wide compositional range (13.4–19.9‰ (qtz equivalent)) denote high isotopic variability within each unit and might reflect the lithologic heterogeneity (i.e., interbedding among sandstones, pelites, and carbonate) evident over tens of meters. Figure 3a illustrates a shift in $\delta^{18}O$ across the sub-Cambrian unconformity, which separates Horsethief Creek rocks from the overlying Hamill Group. Hamill quartzites average 13.0 ± 0.7‰ (qtz equivalent) and possess the lowest signatures in the Dogtooth Range. The Hamill's locally distinctive and homogeneous lithology, pure quartzite (>95% quartz) with minor plagioclase and muscovite, is the simplest explanation for the abrupt decrease in $\delta^{18}O$. Carbonate compositions in the Dogtooth Range are consistent across unit and structural contacts and exhibit a much narrower spread (14.7–17.3‰ (calcite)) than silicates (Figures 3b and 5).

[25] The $\delta^{18}O$ of calcite from wall rocks in the Western Ranges gradually rises with distance up-section and eastward across strike from the Purcell Thrust (Figures 3c and 5). Within calcareous slate and limestone of the McKay Group and its correlative Canyon Creek Formation, calcite exhibits an average $\delta^{18}O$ increase of ~3.0‰ across ~14 km of structural strike, from 17.9 to 20.8‰. Signatures as high as 25.1‰ were documented in the massive dolostones of the Late Ordovician Beaverfoot Formation. However, we focus on the Late Cambrian and Early Ordovician units because of their stratigraphic continuity and lithologic similarity and the relatively narrow time interval over which they were deposited. We emphasize that although centimeter- to meter-scale lithological variations between limestone and calcareous slate are evident, Late Cambrian units in the Western Ranges are dominantly calcareous with differences in bulk carbonate composition generally <10%.

[26] Also, wall rock carbonate compositions at each outcrop in the Western Ranges are distinctly homogeneous with standard deviations that are consistently <0.2‰ (Figure 3c). This implies that the observed regional trend, though subtle, is not an artifact of local, meter-scale variations in composition. That is, because samples of both micrite and calcareous slate (>50% carbonate mineralogy) were collected across 50- to 200-m-wide outcrops, the apparent increase cannot be attributed to minor lithologic changes over tens of meters nor to compositional zoning across millimeters. It is noteworthy that all oxygen compositions from the McKay and Canyon Creek samples fall either below or at the lower end of the 20–24‰ range that typifies global carbonates of similar age [*Veizer*, 1983]. Samples collected east of the Western Ranges from older rocks in the underlying Chancellor Group exhibit values as high as 20.7‰ [*Knoop*, 2000], thus increasing the likelihood that signatures in the McKay and Canyon Creek units are not pristine. We return to these points in section 9 discussion regarding the cause for the observed pattern.

7.2. Regional Distribution of $\delta^{18}O$ in Veins and Vein-Wall Rock Relationships

[27] Here we present isotope data from veins and cataclasites sampled across the transect with specific attention given to vein-wall rock pairs, as well as general observations about the relationship between veins and host rocks at the outcrop-scale (Figures 5a and 5b). In the Dogtooth Range, we observed (1) a narrower range of $\delta^{18}O$ for veins than whole rocks, (2) no association between faults and the magnitude of vein-wall rock disequilibrium, and (3) no systematic relationship between vein and wall rock compositions. No evidence was found for the low-end quartz (12.1–15.0‰) and calcite (6.4–12.7‰) signatures that *Nesbitt and Muehlenbachs* [1997] recorded during their transect through the Proterozoic (Horsethief Creek) units of the northern Purcell Mountains. In fact, the $\delta^{18}O$ of veins lies within the compositional range of rocks sampled at individual outcrops in all but one case and therefore indicates that vein-forming fluids were in approximate isotopic equilibrium with wall rocks.

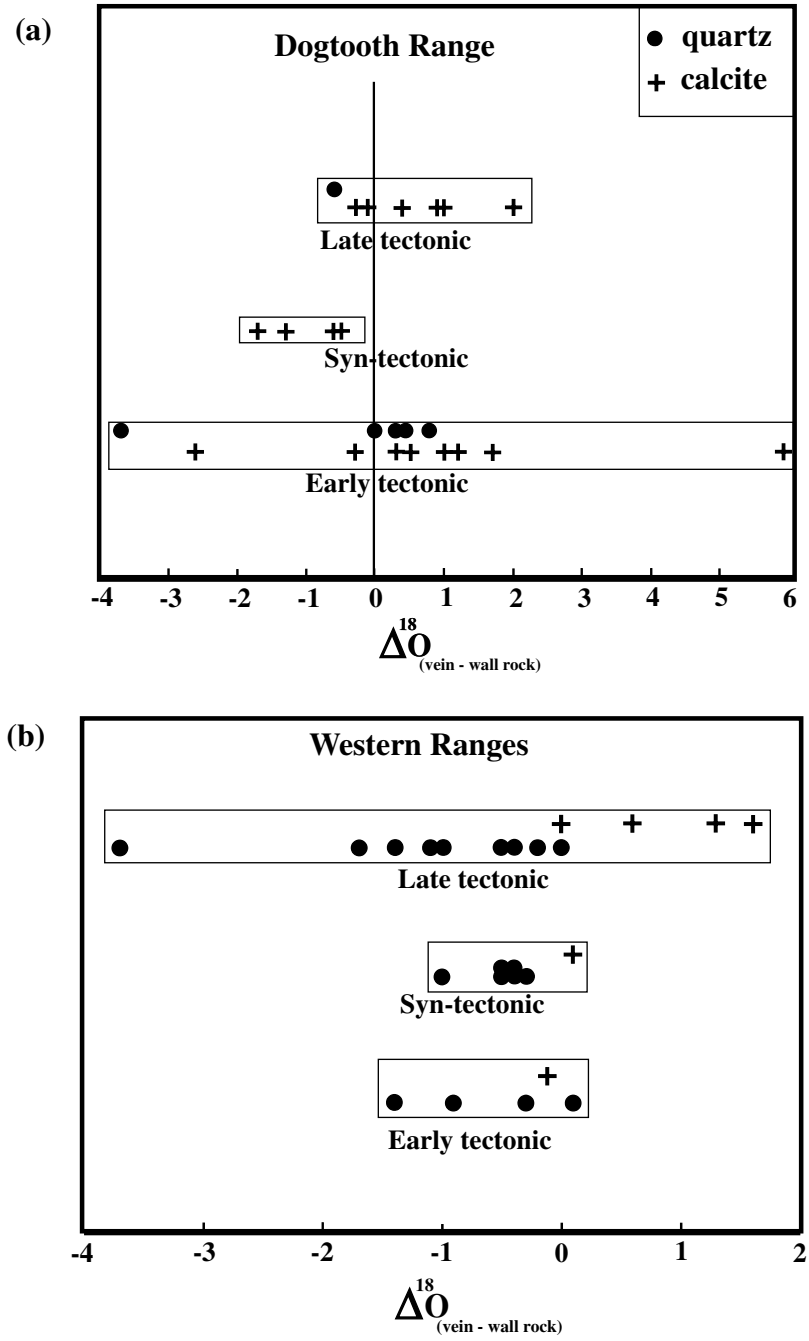

Figure 6. Oxygen fractionation between veins and wall rocks by vein type. The $\Delta_{\text{vein-wall rock}}$ is either δ^{18}O vein calcite-δ^{18}O wall rock calcite (solid circles) or δ^{18}O vein quartz-δ^{18}O wall rock quartz equivalent (crosses). Systematic trends are lacking in both domains, although syntectonic, i.e., cleavage-parallel, veins in the Dogtooth Range are consistently depleted relative to wall rocks.

[28] In the Horsethief Creek Group, the δ^{18}O of quartz veins varies from 14.5 to 19.7‰ compared with that of wall rocks, which lies between 13.4 and 19.9‰ (qtz equivalent)(Table 1). Similarly, quartz veins within the Hamill Group are distributed over a narrower compositional range, 12.5–14.1‰ (excluding an anomalously high value of 18.8‰), than that of their host quartzite, which varies from 12.5 to 14.7‰. In the Dogtooth Range the only evidence for any systematic vein-wall rock disequilibrium occurs within calcite veins from the Horsethief Creek Group, where the range of vein compositions, 13.8–16.3‰, is modestly lower than that of limestone and calcareous shale, 14.7–17.3‰. In section 8.1.2, we argue that this apparent depletion is not indicative of infiltration by externally sourced fluids but instead reflects fluid migration across bedding contacts between siliciclastic and carbonate units.

[29] Compositional differences between veins associated with large-displacement regional faults and their immediate wall rocks are subtle and inconsistent (Figure 6). Of four fault-parallel veins sampled at the Wiseman Creek and Quartz Creek Thrusts, three were enriched by 0.4–1.4‰ and another was slightly depleted by 0.5‰. Furthermore, analysis of vein-wall rock pairs presented in Figure 6 reveals no systematic trend of vein enrichment or depletion in the Dogtooth Range. The fractionation of ^{18}O between veins and wall rocks, $\Delta_{\text{vein-wall rock}}$, varies widely from

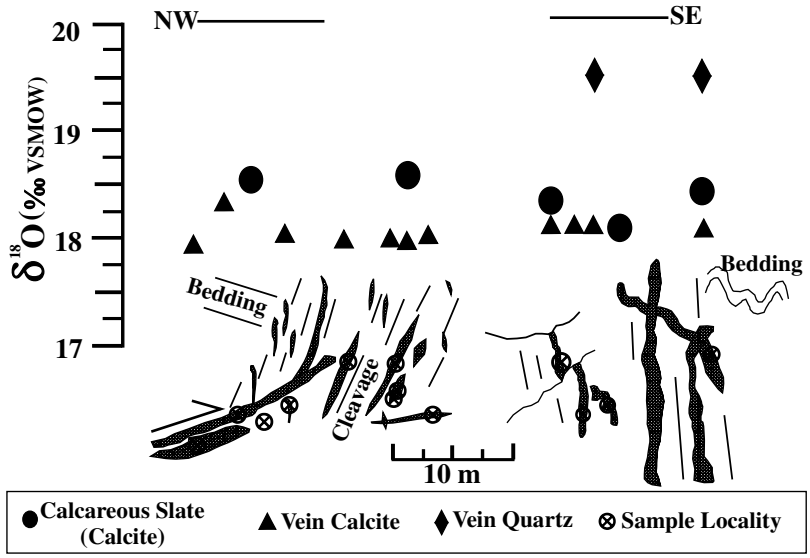

Figure 7. Oxygen isotope values at an outcrop in the Rocky Mountain Trench (outcrop 11) 2.5 km across strike from nearest thrust contact. Despite large temporal and morphological variations, veins are compositionally monotonous and generally lighter than their neighboring wall rocks.

−3.5 to +5.9‰. On the basis of the above evidence that the range in $\delta^{18}O$ of veins is confined within that of wall rocks, the scatter in Figure 6 does not likely reflect multiple fluid regimes throughout the western transect. Instead, we attribute it to wide variation in rock composition at individual outcrops. That is, even though veins might be in apparent disequilibrium with their immediate host rocks, they are still equilibrated with overall bulk rock $\delta^{18}O$ across tens to hundreds of meters (i.e., the minimum distance sampled across each outcrop). We explore this point further in section 8.1.2.

[30] In the Western Ranges, quartz and calcite veins mimic the trend displayed by their host rock carbonate, with a gradual increase in $\delta^{18}O$ eastward and up section from the Purcell Thrust (Figures 5a and 5b). Within Cambrian strata, vein quartz and calcite increase from west to east by 2.5 and 2.1‰, respectively. Therefore the $\delta^{18}O$ of vein-forming fluids in the Western Ranges was at least partially imposed by the composition of dominantly calcareous wall rocks. However, the isotopic relationship between vein calcite and wall rocks is consistently different in the Western Ranges than in the Dogtooth Range. The average $\delta^{18}O$ of calcite veins from Canyon Creek, McKay, and Beaverfoot strata is less than that of wall rock carbonate by 1.6, 1.0, and 2.7‰, respectively (Table 1). Figure 6 illustrates that this depletion, though modest, is systematic and apparent at most outcrops. A maximum depletion of 3.7‰ was documented within a 1-mm-wide veinlet from a cataclasite at an overturned thrust fault along the Trans-Canada Highway (locality 12B, Figure 1). Within the same sample, highly comminuted, very fine grained matrix material is also depleted by 1.1‰ compared with undeformed calcite 2 m away in the hanging wall. Similar style breccias from the two other fault zones that were sampled exhibited a $\Delta_{\text{vein-wall rock}}$ of ∼1.0‰ (localities 12A and 13). Of 21 vein-wall rock pairs, oxygen enrichment (+0.1‰) was observed within only one calcite vein.

[31] The magnitude of depletion is independent of vein type (Figure 6). This phenomenon is best illustrated at an outcrop in the Rocky Mountain Trench ∼4 km east of the Purcell Thrust (Figure 7). Vein density at this locality is unusually high (10–20%), and at least five distinct generations of veins are associated with numerous meter-scale reverse faults. Despite evidence that vein precipitation progressed from early (tightly folded, bedding-parallel veins) into late (laminated, fault-parallel veins) tectonism, 12 samples from across 50 m demonstrate a remarkable uniformity in composition from 17.8 to 18.3‰. With the exception of a single sample of micrite that possesses a slightly lower $\delta^{18}O$ (−0.1‰) than a neighboring vein, wall rocks consistently exhibit larger signatures than the veins with which they are in contact by 0.2–0.8‰.

[32] To summarize, vein-forming fluids were modestly, but systematically, displaced from isotopic equilibrium with surrounding carbonates in the Western Ranges. Depletions occur within all types of synkinematic veins, regardless of their geometry or timing relative to the main phase of tectonism. However, it is noteworthy that cataclasite from a regional fault exhibited the largest departure from equilibrium. These observations support: (1) the presence of a fluid component that was partially exotic to the bulk rock isotopic system at each outcrop, (2) the presence of a locally sourced fluid that equilibrated with lower-$\delta^{18}O$ silicate phases, and/or (3) a situation of prevailing kinetic or thermal disequilibrium between vein-forming fluids and wall rocks.

7.3. Quartz-Calcite Isotope Thermometry

[33] Oxygen isotope thermometry was applied to nine quartz-calcite pairs that appeared to have coprecipitated in veins across the transect (fractionation factors from *Sharp and Kirschner* [1994]). Results are presented in Figure 8. For the most part, these data are compatible with calcite-dolomite solvus thermometry performed on wall rocks in the Dogtooth Range [*Kubli*, 1990] and a portion of the Western Ranges ∼15 km north of the study area [*Gardner*, 1977]. The isotope data yield vein temperatures that range between 305°C and 420°C. Veins in which quartz and calcite clearly showed a crosscutting relationship with each other gave predictably unrealistic temperatures. In addition, two measurements taken within a meter of each other on the same fault-parallel vein at the Purcell Thrust (34-5A/B) gave discordant temperatures of 420°C and 315°C. We suggest that the former value is unrealistically high because of isotopic disequilibrium between quartz and calcite at the thrust contact. Calcite-dolomite solvus thermometry of *Knoop* [2000] yielded a range of 260–350°C from a single fibrous vein (17-3E) adjacent to the Heather Mountain Thrust and a maximum temperature of 290°C from a breccia-hosted veinlet (36-1B) in the Western Ranges (for

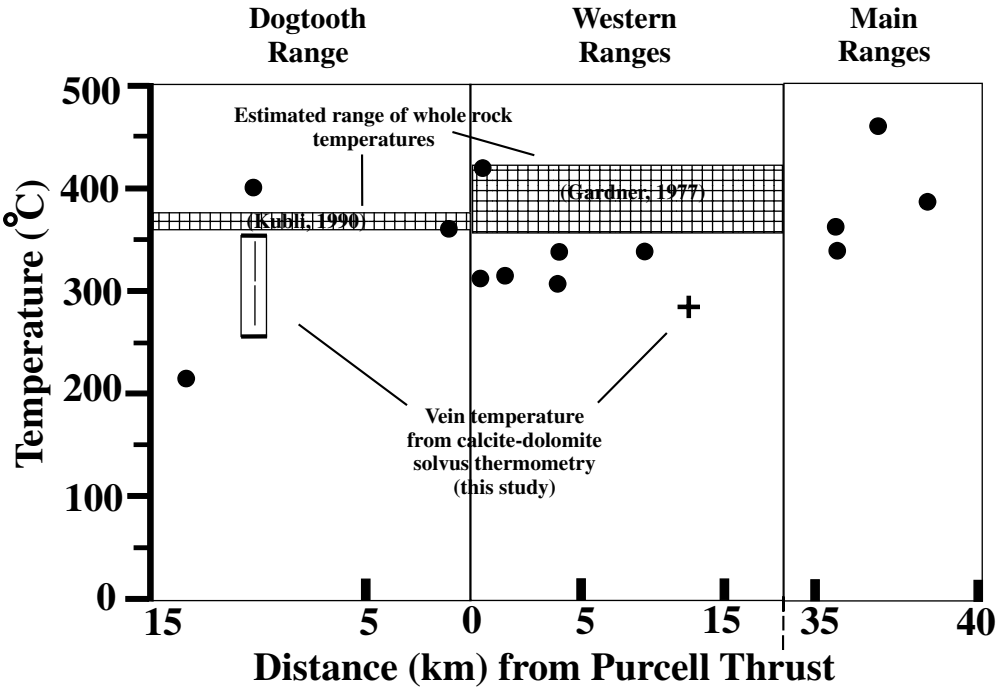

Figure 8. Estimated temperature of quartz-calcite veins from isotope and calcite-dolomite solvus thermometry. Fractionation factors for quartz-calcite taken from *Sharp and Kirschner* [1991]. Calcite-dolomite thermometry based upon data from *Knoop* [2000] and thermometer of *Anovitz and Essene* [1987].

methodology, see *Anovitz and Essene* [1987]). Isotope thermometry on 17-3E yielded a temperature of 400°C.

8. Discussion

8.1. Potential Catalysts for Isotopic Depletion

[34] Anomalously low $\delta^{18}O$ (carbonate) values in the Dogtooth and Western Ranges and systematic depletions in vein calcite relative to wall rocks suggest several possible scenarios (Table 2). Specifically, these include (1) the age dependence of carbonate $\delta^{18}O$, in accordance with the tendency of older rocks to possess lower oxygen values, (2) exchange with low-$\delta^{18}O$, metamorphic fluids that were sourced from coexisting clay minerals during devolatization reactions, (3) localized, fluid-assisted isotopic exchange with coexisting, lower-$\delta^{18}O$ phases such as quartz and muscovite, (4) down-temperature (i.e., up section) flow of a fluid that was isotopically equilibrated but hotter than surrounding wall rocks such that the veins which precipitated exhibited lower $\delta^{18}O$ than their host rocks, (5) exchange with a fluid that was in thermal and isotopic equilibrium with wall rocks and flowed up a temperature gradient (i.e., down-section), and (6) exchange with an exotically derived, low-$\delta^{18}O$ fluid. Disequilibrium dissolution of wall rock and H_2O-CO_2 immiscibility during vein formation have also been cited as catalysts for depletions in fluid $\delta^{18}O$ [*Cartwright et al.*, 1994]. We regard these as second-order factors due to the (1) lack of evidence for large temperature and pressure fluctuations during veining, (2) variability in degree of disequilibrium documented in veins, and (3) systematic enrichment in vein $\delta^{13}C$ compared to wall rocks (Tables A1 and A2) and not a $\delta^{13}C$ depletion as would result for fluid immiscibility [*Cartwright et al.*, 1994].

[35] Using specific examples from individual outcrops, the following sections incorporate a more detailed analysis of the isotopic data in order to identify the scenarios that best apply to syntectonic fluid regimes in the Dogtooth and Western Ranges.

8.1.1. Possible age controls on wall rock $\delta^{18}O$ (calcite). [36] The pattern of westward and down-section $\delta^{18}O$ depletion in veins and rocks does not conform to the statistical model of *Veizier and Hoefs* [1976], who noted that Late Proterozoic and Phanerozoic carbonates follow a well-constrained trend of declining $\delta^{18}O$ with increasing age. In the Dogtooth Range, *Ghent and O'Neil* [1985] recorded an oxygen value of ~21‰ from a marble protolith in the Horsethief Creek Group, and *Veizier and Hoefs* [1976] predict a $\delta^{18}O$ of 22–22.5‰ for carbonates of similar age. Therefore calcite and dolomite, which possess an average signature of 15.6 ± 0.8‰ in the Dogtooth Range, have likely undergone secondary exchange with depleted fluids or exchange with coexisting low-$\delta^{18}O$ phases via diffusion.

[37] In the Western Ranges the composition of wall rocks from the Canyon Creek and McKay units falls either below or at the lower end of typical carbonates of similar age. For the maximum possible duration of deposition of these sediments (527-487 Myr), *Veizier and Hoefs* [1976] predict a $\delta^{18}O$ decrease of 0.2–0.5‰ with increasing age. Thus the observed 3.0‰ decrease across the Western Ranges cannot be explained by age variation and must instead reflect interaction with a low-$\delta^{18}O$ fluid. Apparent isotopic exchange is greatest in the west, where signatures near the Purcell Thrust exhibit a maximum departure from the expected $\delta^{18}O$ of Upper Cambrian carbonates (Figures 5a and 5b).

8.1.2. Fluid regimes in the Dogtooth Range. [38] An obvious local reservoir for the low-$\delta^{18}O$ fluid in the Dogtooth Range is the abundant siliceous sandstone and metapelite present at each sample locality. Consistent with the notion of isotopic homogenization throughout the Horsethief Creek section, we contend that local fluid advection across at least tens of meters (i.e., the maximum bed thickness for limestone) promoted exchange between siliciclastic rocks and subordinate carbonates, thereby lowering the $\delta^{18}O$ of carbonate wall rocks. In this section we illustrate that the tendency of vein signatures to approach that of the

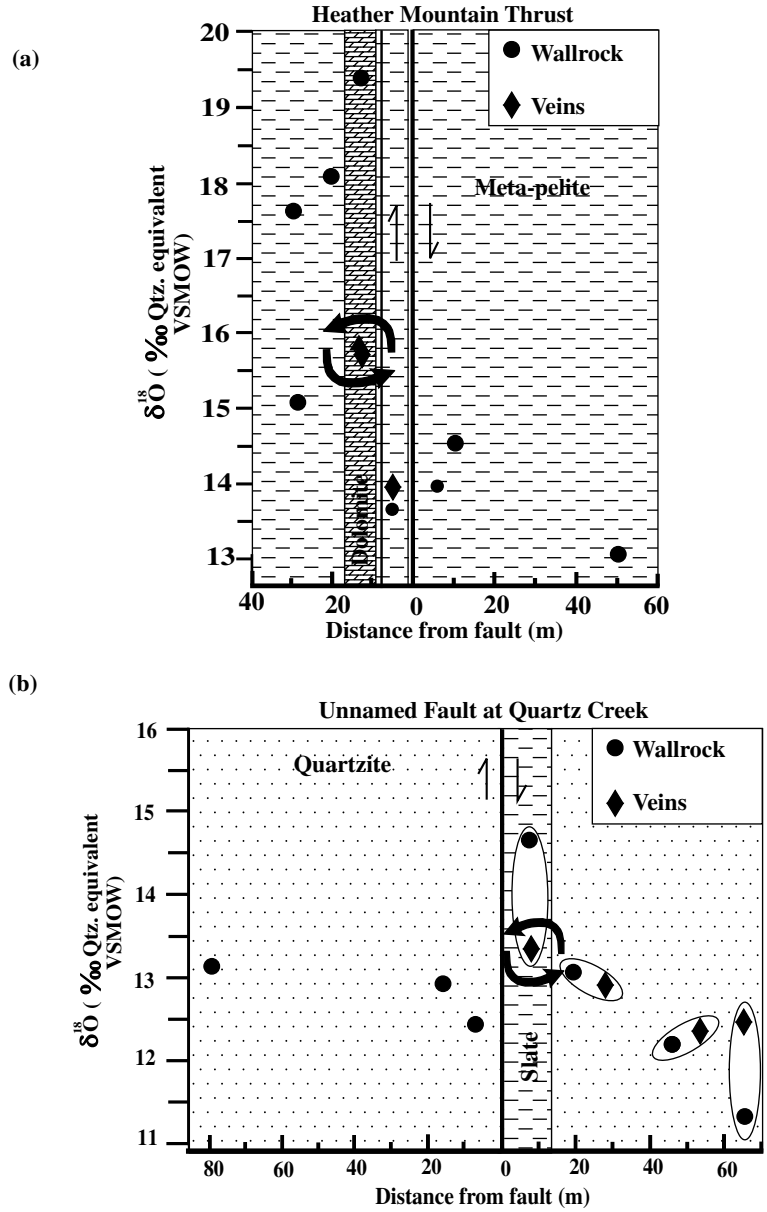

Figure 9. Isotopic evidence for fluid migration across bedding contacts and meter-scale homogenization at outcrops in the Dogtooth Range. Solid circles denote wall rocks, diamonds denote quartz veins, and triangles denote calcite veins. (a) A quartz-calcite vein exhibiting signatures that are intermediate between the host dolomite and the more abundant metapelite. (b) A quartz vein exhibiting a signature that is intermediate between the host slate and the surrounding quartzite.

average wall rock $\delta^{18}O$ provides another line of evidence to support fluid advection across $\geq$10 m. In discussion we restrict the size of the fluid-rock system to the limits of sampling, i.e., individual outcrops ($\leq$100 m), although obviously it might be larger (e.g., the distance to the next outcrop sampled). Use of the terms closed and open system therefore refers to respective conditions of geochemical "isolation" versus exchange between outcrops.

[39] Isotopic disequilibrium between veins and their immediate host rocks provides further evidence for fluid migration across bedding contacts. At the Heather Mountain Thrust (locality 1), a 1-cm-wide, antitaxial quartz-carbonate vein is depleted relative to its host dolomite by ~3.5‰ (Figure 9a). Thirty centimeters away, a quartz-arenite unit borders the dolomite and possesses a lower $\delta^{18}O$ of 13.8‰ (qtz equivalent). Transport of fluid between the dolomite and sandstone best explains the intermediate oxygen value possessed by the vein (i.e., scenario 3 in section 8.1). Otherwise stated, the vein-forming fluid had undergone isotopic exchange with both the sandstone and dolomite. Thus the time-integrated fluid flux was sufficiently low to permit rock buffering of the silica and carbonate-bearing species such that the signature of vein quartz and calcite approached that of the average bulk rock package (i.e., dolomite + quartz arenite). Although quartz precipitation by chemical diffusion has been documented in crack-seal veins [*Fisher and Brantley*, 1992], diffusion across more than a few centimeters is relatively inefficient [*Etheridge et al.*, 1984], making advection the most viable transport mechanism for the $\delta^{18}O$-depleted fluid.

[40] Figure 9b illustrates a similar phenomenon within a fibrous, cleavage-parallel vein at an unnamed thrust fault in the

central Dogtooth Range (locality 6). The vein, which is depleted by 1.3‰ compared with surrounding wall rock, is hosted by a 10-cm-wide phyllite that is isolated within an outcrop of quartzite. However, the vein is nearly equilibrated with nearby quartzite, and therefore precipitated from a fluid that was almost entirely buffered by the dominant rock type within the outcrop.

[41] Finally, a comparison between whole rock and vein signatures across the same outcrop reinforces the assertion that centimeter- to meter-scale fluid flow homogenized vein compositions in the western transect. The $\delta^{18}O$ of wall rocks in Figure 9b ranges from 11.5 to 14.7‰, while vein quartz is more narrowly distributed between 12.5 and 13.4‰. In fact, with the exception of a single, anomalously high-$\delta^{18}O$ quartz vein (18.8‰), vein signatures at each outcrop sampled in the Dogtooth Range fell within the range of those for wall rocks [*Knoop*, 2000]. This subdued variation in the composition of veins and simultaneous disequilibrium between veins and their immediate host rocks (i.e., Figure 6) suggests that vein-forming fluids had been in contact with wall rocks located at least a few, but possibly tens to hundreds of meters away from the site of quartz precipitation. The above examples support a scenario in which the $\delta^{18}O$ of veins, though in modest disequilibrium with the immediate host rock, approach the average bulk rock composition across at least a few meters. Thus, although a pervasive or channeled open-system fluid regime is possible, it need not be invoked to explain the observed patterns in isotope composition.

8.1.3. Fluid regimes in the Western Ranges. [42] The next section expands upon and tests the above scenarios for closed and open system fluid-rock exchange in the Western Ranges. Data from wall rocks and veins are discussed separately.

8.1.3.1. Local fluid circulation in a closed system: [43] Under these conditions, isotopic alteration and dissolution-reprecipitation reactions are restricted to the preexisting rock-fluid system, with no influx of fluid or solutes from external sources. In section 8.1.1 we refuted the notion that age variation is responsible for increasing wall rock depletion westward toward the Purcell Thrust, and we must therefore propose a secondary process capable of altering and homogenizing rock compositions. Dehydration reactions, which occur during the formation of chlorite and muscovite from clay minerals, are capable of generating a substantial volume of fluid during regional metamorphism and cleavage development [e.g., *Etheridge et al.*, 1984; *Valley*, 1986; *Ferry*, 1992]. For example, *Ferry* [1992] estimated that Appalachian metacarbonates of similar grade to those in the Western Ranges experienced a time-integrated fluid flux of 4.0×10^2 mol H_2O cm^{-2} during regional metamorphism. Pervasive circulation of locally derived metamorphic fluid can produce systematic carbonate depletions by (1) promoting isotopic exchange between carbonates and coexisting, lower-$\delta^{18}O$ siliceous phases (i.e., scenario 3 above) or (2) promoting isotopic exchange between carbonates and the metamorphic fluid itself (scenario 2). If either of these were the catalyst for the observed depletions, then outcrops with the lowest carbonate $\delta^{18}O$ should possess the highest silicate content.

[44] Figure 10a plots carbonate $\delta^{18}O$ against silicate content for samples in the McKay Group and Canyon Creek Formation. In five of six samples, where $\delta^{18}O$ varies over 2.5‰, silicate abundance varies by <15%. The one sample with substantially higher carbonate content (~80%) has $\delta^{18}O$ that is only 0.5‰ higher than the top end of the range defined by the other five samples. As a group, these data fail to show a consistent, positive correlation between abundance and oxygen isotope composition of calcite. Moreover, the McKay Group and Canyon Creek Formation are massive and homogeneous in outcrop relative to the siliciclasitic rocks of the Dogtooth Range. The McKay Group and Canyon Creek Formation lack the distinct low ^{18}O reservoirs (e.g., quartzite or metapelite) that appear to drive ^{18}O depletion in veins during outcrop scale fluid circulation in the Dogtooth Range (Figure 9). We therefore dismiss the effect of local bulk rock composition (over centimeters to tens of meters in scale) in producing $\delta^{18}O$ depletion within the calcite of wall rocks.

[45] We have demonstrated that syntectonic carbonate veins from the Western Ranges are systematically depleted relative to their wall rocks. The regularity of this pattern and the lack of corresponding enrichment preclude the effects of random kinetic disequilibrium between rocks and fluid as being the cause for isotopic discrepancies between veins and wall rocks. As previously stated in section 4, peak metamorphism in the Western Ranges was broadly coeval with the main phase of deformation and vein development. If the hydrous phases were isotopically lighter than surrounding carbonates and the residence time of the metamorphic fluids was sufficiently brief to prevent homogenization with wall rocks, the resultant veins will exhibit a lower $\delta^{18}O$ than that of wall rock calcite [*Valley*, 1986]. Under such conditions a correlation between hydrous mineral abundance and magnitude of vein depletion is expected. Figure 10b illustrates that no such correlation exists. In fact, the two largest depletions occur in dolomite and limestone breccia from outcrops that contain <5 mol % hydrous minerals. Hence closed system cycling of metamorphic fluid between sites of devolitization reactions and open fractures cannot fully explain systematic fluid-rock disequilibrium across the Western Ranges.

[46] Systematic vein depletion within an isotopically closed system can also result from thermal disequilibrium between wall rocks and fluids (scenario 4). The fractionation of ^{18}O between water and calcite during vein precipitation is a temperature-dependent process that is quantifiable by a partition coefficient. Fluids that are isotopically equilibrated with the rocks through which they pass can nevertheless produce relatively low-$\delta^{18}O$ veins if they are hotter than surrounding rocks [e.g., *Lee et al.*, 1997]. Assuming an ambient temperature of 350°C, depletions of 1.0‰ are possible in veins that precipitated from fluids elevated by 50–60°C [*O'Neil et al.*, 1969; *Zheng*, 1999]. Given a geothermal gradient of 30°C km^{-1}, this requires that fluids ascending from a minimum of ~1.7–2 km below the dilation site traveled at rates high enough to prevent cooling. For fluid fluxes typical in metamorphic environments ($<10^{-9}$ m s^{-1}), conduction has been shown to outweigh advection as a mechanism for heat transport [e.g., *Bickle and McKenzie*, 1987], making thermal perturbations from long distance fluid flow unlikely. Even for large fluxes of $\sim10^{-8}$ m s^{-1} that are confined to within shear zones, modeling predicts that the temperature of an ascending fluid will only be ~26°C hotter than the host rock [*Dipple and Ferry*, 1992a]. Distributed flow through a fracture network will result in even more subdued thermal perturbation [*Brady*, 1988]. Furthermore, vein temperatures deduced from isotope thermometry are consistently between 300°C and 350°C and therefore are compatible with the estimated ambient rock temperature. We conclude that localized fluid migration on a scale of 100 m or less fails to account for (1) the low $\delta^{18}O$ of carbonates and (2) systematic differences between vein and wall rock calcite in the Western Ranges.

8.1.3.2. Fluid flow up temperature: [47] Although up-temperature fluid migration is a potential mechanism for lowering the isotopic composition of wall rocks, the absence of extensional faults and low rock permeabilities make it unlikely that the requisite large volumes of fluid were siphoned downward against a lithostatic pressure gradient. Transport theory dictates that under conditions of thermal and kinetic equilibrium exchange between water and rock, fluid migrating up a temperature gradient, i.e., downward through a stratigraphic package or along a fault, will drive $\delta^{18}O$ values downward [*Dipple and Ferry*, 1992b; *Bowman et al.*, 1994]. The magnitude of these shifts is a function of the time-integrated fluid flux and the profile of the geothermal gradient. On the basis of the one-dimensional transport model of *Dipple and Ferry* [1992b], time-integrated fluid fluxes of

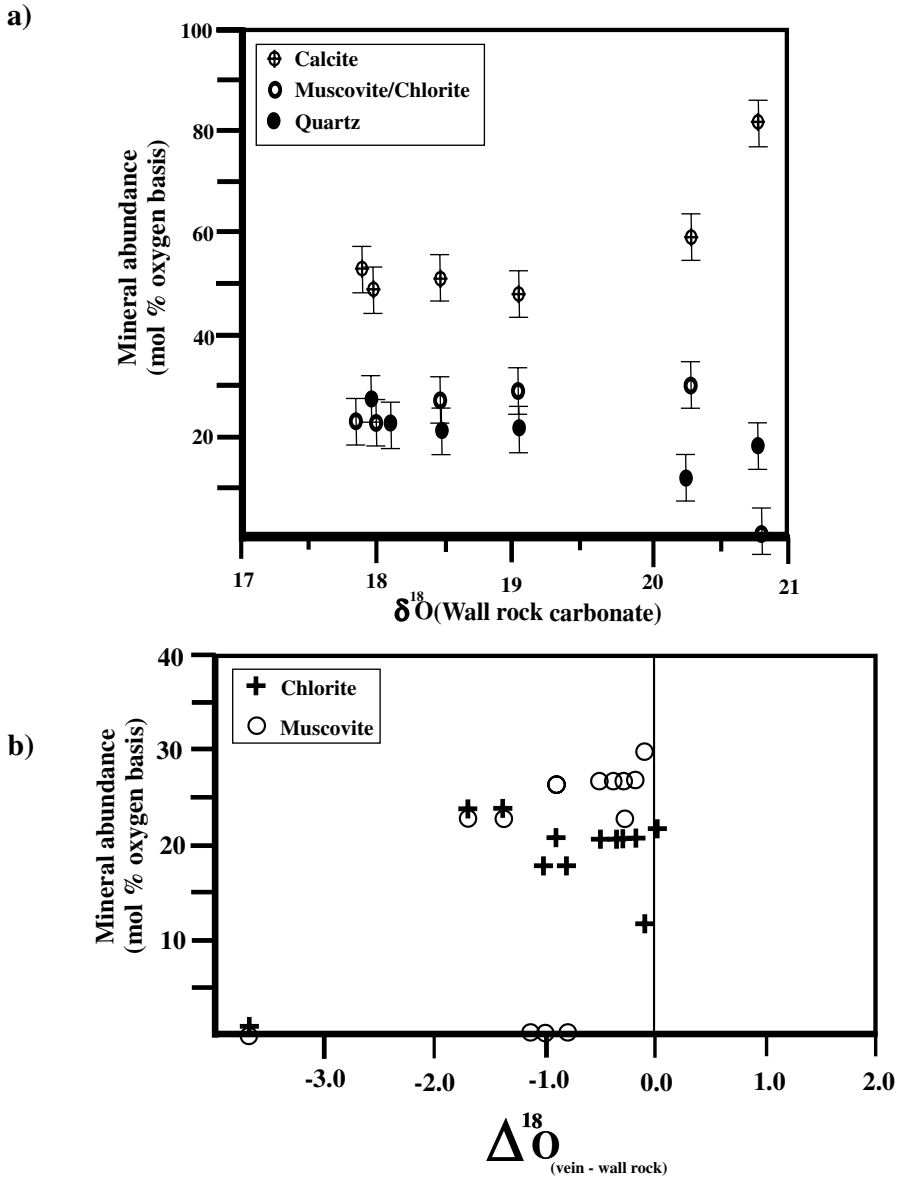

Figure 10. (a) Mineral abundance versus mean isotopic signature for Canyon Creek and McKay outcrops in the Western Ranges. With the exception of the two easternmost outcrops, a correlation between calcite and oxygen composition is lacking. (b) Mineral abundance versus vein-wall rock fractionation by sample. The magnitude of depletions does not correlate with silicate composition, as would be expected if vein signatures were rock buffered. The mol % oxygen basis is moles O in mineral/moles O in rock.

$\sim 1-4 \times 10^4$ mol H_2O cm^{-2} over a path length of 1–5 km and across a geothermal gradient of +30°C km^{-1} will lower the $\delta^{18}O$ of wall rocks by 1–3.7‰. Some studies have documented the siphoning of such large volumes of shallow fluid downward against a lithostatic gradient [*Burkhard and Kerrich*, 1988; *McCaig*, 1988; *Cartwright and Buick*, 1999]. For example, *Cartwright and Buick* [1999] used silica solubility to estimate a time-integrated fluid flux of 2.1×10^6 mol H_2O cm^{-2} in ductile shear zones of the Alice Springs Orogen. However, most of these models invoke the channeling of fluids along high strain zones, such as mylonites, or demand a latent phase of stress relaxation and extensional faulting to justify fluid migration up a pressure gradient. Neither of these situations applies to localities in the Western Ranges. A more reasonable mechanism for promoting systematic vein depletion is the large-scale influx of fluid from a low-$\delta^{18}O$ source.

8.1.3.3. Open-system fluid regime: An eastward migrating isotopic front: [48] On the basis of the absence of credible closed system processes, we advocate a scenario of kilometer-scale fluid infiltration across the Western Ranges during Mesozoic contraction resulting in depleted wall rock compositions and disequilibrium between veins and wall rocks (Figure 11). We argued in section 8.1.2 that a factor other than local homogenization between silicates and calcite is responsible for the westward decrease in $\delta^{18}O$. The most plausible alternative to this is the pervasive eastward flow of relatively low-$\delta^{18}O$ fluids across the transect and the subsequent reequilibration of host rocks. Evidence for this is provided by the outcrop from the Rocky Mountain Trench depicted in Figure 7. The density of fractures and faults is higher here (~10–20%) than at any other locality, wall rocks possess the lowest $\delta^{18}O$ of all carbonates sampled from the McKay Group, and oxygen values across the outcrop are

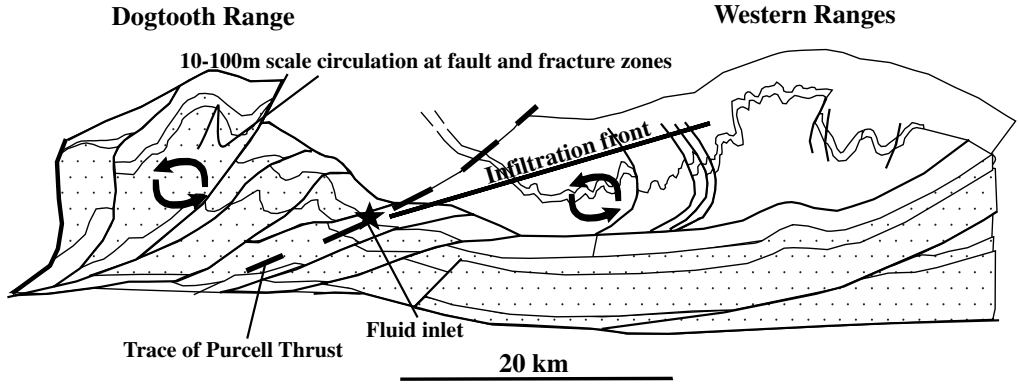

Figure 11. Proposed scenario of both local and large-scale fluid migration (denoted by infiltration front) in the Dogtooth and Western Ranges. Configuration of study area follows initial phase of deformation but prior to displacement on Purcell Thrust. Fluid inlet used for modeling is chosen as contact between the Donald Formation and Chancellor Group at the trace of the Purcell Thrust. Stippled units are predominantly siliciclastic, and open units are predominantly calcareous. Modified from *Kubli and Simony* [1994].

remarkably uniform. Elevated permeability from an interconnected network of microscale and mesoscale fractures apparently promoted efficient fluid flow and homogenization within the outcrop and also permitted greater access to externally derived fluids (e.g., fault fracture meshes from *Sibson* [1996]).

[49] An ascending, eastward migrating, low-$\delta^{18}O$ fluid, which infiltrated Canyon Creek and McKay sediments from the west, could generate the observed pattern of whole rock depletion across a flow path $\geq$14 km. The gradational nature of the profile is consistent with substantial fluid dispersion and/or retarded exchange kinetics during the flow event. Siliciclastic sequences in the Dogtooth Range represent an obvious, low-$\delta^{18}O$ reservoir from which this isotopic front could have been derived. We therefore propose that low-$\delta^{18}O$ fluid was either expelled or siphoned from the Dogtooth Duplex during contraction and migrated eastward and up section into the carbonate sequences of the Western Ranges, where it produced a wide zone of isotopic depletion. A sample of calcareous siltstone from the Donald Formation, the shallowest and easternmost unit west of the Purcell Thrust, exhibits a signature of 16.0‰ (calcite) and best approximates the composition of rocks in equilibrium with fluids at their point of entry into the Middle and Upper Cambrian sequence.

[50] The observed departure from equilibrium within veins is small enough to necessitate substantial buffering of fluids by wall rocks. However, the systematic nature of these depletions suggests that vein-forming fluids exchanged only partially with wall rocks and therefore retained a light isotopic component from the source. In this scenario the magnitude of vein depletion reflects the extent of disequilibrium between rock and fluid.

[51] It is beyond the scope of this study to constrain the exact mechanisms by which fluids were transported across the Western Ranges. Substantial isotope depletions as high as 3.7‰ at thrust faults suggest that fault zones experienced greater time-integrated fluid fluxes than fracture networks within thrust sheets. However, three of the four McKay outcrops (including that in Figure 7) were at least 2.2 km across strike from the nearest kilometer-scale thrust fault, making it unlikely that major thrusts and related fractures were the only principle conduits through which exotic fluids were supplied to these rocks. A spaced, penetrative cleavage is pervasive throughout the Western Ranges, and centimeter-spaced stylolitization is common within more competent limestone and dolomite. Numerous studies have emphasized the ability of secondary cleavage to raise rock permeability through volume loss and microcracking by an order of magnitude >5 [e.g., *Etheridge et al.*, 1984; *Cox and Etheridge*, 1989; *Sibson*, 1996]. Others have demonstrated that cleavage planes and stylolites can focus fluids across more than or equal to hundreds of meters [*Bradbury and Woodwell*, 1987; *Rye and Bradbury*, 1988]. Given the extensive evidence for pressure solution, recrystallization, fracturing, and meter-scale faulting at each outcrop, it is a reasonable assumption that deformation and attendant metamorphism actively enhanced permeability and promoted fluid migration throughout the Western Ranges. The absence of a similar isotopic front in the Dogtooth Range indicates that fluid-rock exchange, though active at the outcrop scale, was not necessarily as extensive in deeper levels west of the Purcell Thrust. This is compatible with the above scenario if (1) the siliceous sediments of the Dogtooth Range were the source of upwelling metamorphic fluid that was expelled into the Western Ranges and (2) fluid channeling along regional faults in the Dogtooth Range, as opposed to pervasive flow along cleavage and local fault fracture networks, was the dominant mechanism by which distally sourced, isotopically depleted fluids were supplied to rocks in the Western Ranges.

8.2. Model-Derived Constraints for Time-Integrated Fluid Flux and Kinetic Dispersion

[52] The variation in $\delta^{18}O$ of rocks and veins with distance to the Purcell Thrust (Figures 5a and 5b) resembles alteration patterns that are predicted by reactive transport models for coupled fluid flow and isotopic exchange. These models predict that flow of isotopically light fluid from the Dogtooth Range into the Western Ranges (scenario 6) would produce a zone of ^{18}O depletion immediately downstream of the contact between the two rock packages. In some instances, the zone of depletion is a distinct trough bounded on the downstream side by a sharp geochemical front, but in many natural occurrences the geochemical front is broadened and rounded by a variety of physical and chemical processes that are collectively referred to as hydrodynamic dispersion (Figure 12). Dispersion in crustal environments has been attributed to sluggish reaction kinetics between rock and fluid (kinetic dispersion [e.g., *Lassey and Blattner*, 1988; *Bickle*, 1992]), heterogeneous fluid flow (kinematic dispersion [e.g., *Bowman et al.*, 1994]) or to simultaneous chemical reactions with coupling between chemical systems (reaction dispersion [*Dipple*, 1998]).Dispersive effects of diffusion are typically limited to length scales of a few meters or less [*Bickle and McKenzie*, 1987].

8.2.1. Model description and assumptions. [53] We employ a one-dimensional model of reactive transport of oxygen isotopes for comparison to the $\delta^{18}O$ profiles from the Western Ranges. In adopting a one-dimensional model we are assuming that the dominant direction of fluid flow was parallel to the axis of

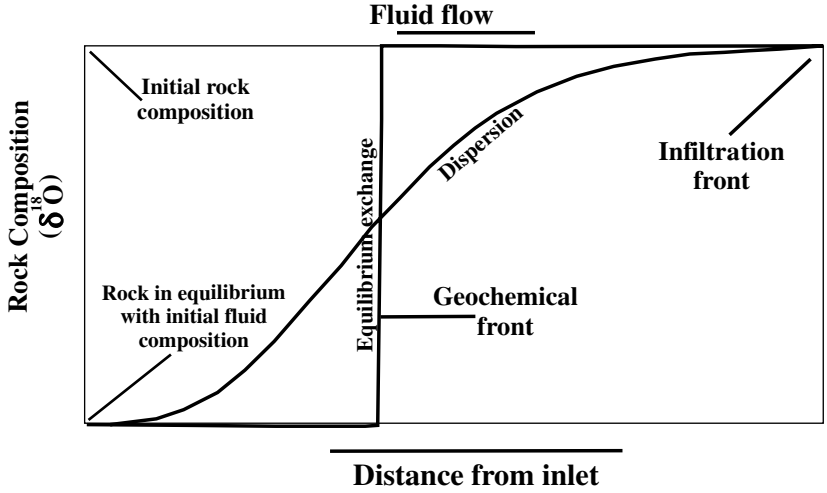

Figure 12. Comparison of equilibrium ($N_D = \infty$) versus disequilibrium ($N_D < 100$) fluid-rock isotope exchange for the infiltration of a low-$\delta^{18}O$ fluid through a homogeneous, isothermal rock volume. Slow kinetics result in a broadened geochemical front (GF), whereas an abrupt geochemcial front develops under equilibrium conditions. Isotope compositions to the left of the GF nearer the inlet are fluid buffered, and those to the right are rock buffered.

the transect, which is a diagonal flow path eastward and up section along fault fracture and cleavage networks. We infer this because the Dogtooth Range represents both a westward locus of deformation and the most reasonable source of isotopically depleted fluids. We also assume that the dominant direction of fluid flow was subparallel to the structural fabric as it was oriented during the onset of contraction, i.e., southwest dipping and northeast vergent [cf. *Logan*, 1992; *Oliver*, 1996]. We cannot thoroughly exclude the possibility that fluids migrated vertically upward into the Western Ranges from an underlying siliciclastic reservoir. If true, the flow path was shorter by less than one half the distance incorporated into the lateral flow model.

[54] We further assume that the principle fluid flow and alteration event transpired prior to displacement on the Purcell Thrust. The main phase of deformation and synkinematic vein development in the Dogtooth and Western Ranges predated motion on the Purcell Thrust (PTF) by an indeterminate amount of time. Therefore an appropriate $\delta^{18}O$ versus distance profile should reflect the tectonic configuration prior to displacement on the PTF. *Kubli and Simony* [1994] have provided the only published cross section with restored movement on the PTF (Figure 11), and it is to this section that data from the Dogtooth and Western Ranges are coupled when depicting the most reasonable distribution of $\delta^{18}O$ that immediately followed the proposed syn-D1 event. Distances are measured from a hypothetical fluid inlet located at the contact between the Donald Formation and the lower Chancellor unit where it crosses the trace of the PTF (Figure 11). Simulations that assume a post-Purcell Thrust fluid event shorten the path length to ~14 km. To summarize, the fluid flow path illustrated in Figure 11 and adopted below assumes that most fluid flow occurred in the direction of the dominant structural fabrics and before activation of the Purcell Thrust. If either or both of these assumptions in incorrect, then the alteration profile would be shortened by ~40% and our estimates of time-integrated fluid flux would decrease by a factor of ~2. Shortening of the alteration profile would also sharpen the alteration profile, reduce the amount of dispersion, and increase inferred reaction rates [see *Knoop*, 2000].

[55] We adopt the reactive transport model of *Lassey and Blattner* [1988], which attributes dispersion to sluggish reaction kinetics because (1) oxygen isotope exchange kinetics between fluid and carbonate and silicate minerals is relatively sluggish at the modest temperatures attained in the Western Ranges [*Cole and Ohmoto*, 1986] and (2) simultaneous sampling of wall rock and vein provides information on the variation of rock and fluid composition along the transect. The systematic differences in rock and vein composition in the Western Ranges (Figures 6b and 7) is an important constraint for our reactive transport modeling because it demonstrates that fluid and rock were out of local isotopic equilibrium. However, by attributing all dispersion to reaction kinetics we are neglecting other mechanisms of dispersion and our constraints on reaction rates are therefore minimum estimates. Estimates of time-integrated fluid flux are not sensitive to this assumption because the manifestation of other mechanisms of dispersion is similar to that produced by the Lassey and Blattner model and because, as we demonstrate below, estimates of time-integrated fluid flux are not strongly sensitive to variations in the amount of dispersion if model results are compared to the data in a least squares sense.

[56] *Lassey and Blattner* [1988] derived an analytical solution to the dimensionless equations for mass balance (equation (1)) and kinetic (equation (2)) exchange:

$$\partial/\partial\tau\left(\Phi'\delta^{18}O_{water} + \delta^{18}O_{rock}\right) + \Phi'\partial/\partial Z\delta^{18}O_{water} = 0 \qquad (1)$$

$$\partial/\partial\tau\delta^{18}O_{rock} = N_D\left(\alpha\delta^{18}O_{water} - \delta^{18}O_{rock} + \Delta\right), \qquad (2)$$

where τ is dimensionless time since commencement of infiltration (= tq/L; q is the mean longitudinal interstitial (Darcy) velocity; L is the length of infiltrated aquifer); Φ' is the ratio of oxygen in pore-bound fluid to that in rock; Z is the dimensionless position in the aquifer; α represents isotopic fractionation between phases; $\Delta = 10^3(\alpha - 1)$; and Damköhler number ($N_D$) = $\kappa L/q$. The Damköhler number essentially reflects the ratio between the rate constant for ^{18}O exchange between water and rock, κ, and flow rate, q. Large values of N_D correspond to a closer approach to chemical/isotopic equilibrium.

[57] Our formulation of the *Lassey and Blattner* [1988] solution was implemented in FORTRAN and employs an algorithm from *Lassey* [1982] for evaluating the K function in equations (5a) and (5b) of *Lassey and Blattner* [1988]. The model assumes isothermal fluid flow at 370°C, corresponding to a $\Delta_{calcite\text{-}water}$ of 3.8‰ [*O'Neil et al.*, 1969]; initial fluid and rock compositions of 12.2‰ (≈16.0‰$_{(calcite)}$ at 370°C) and 21.0‰, respectively; permeable porosity of 0.05; and a molar H_2O volume of 22 cm^3

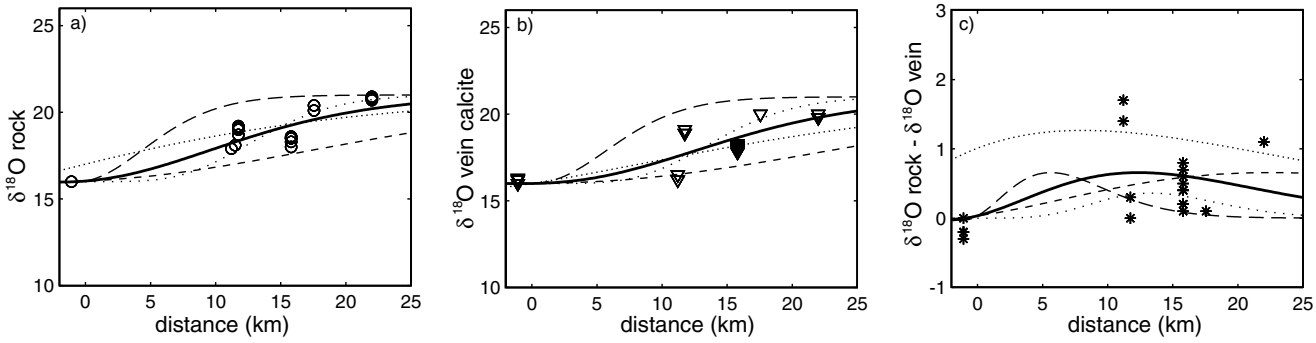

Figure 13. Oxygen isotope compositions of carbonate (a) whole rocks, (b) calcite veins, and (c) the difference of rock and vein. Measurements are plotted as data points, and model results are plotted as curves. The solid curve is the best fit solution to the data in a least squares sense and results from infiltration of time-integrated fluid flux of 1.1×10^5 mol H_2O/ cm^2 and a Damköhler number of 5. The best fit was determined by comparing the model curve to the whole rock and wall rock-vein pair data (Figures 13a and 13c). The dashes curves illustrate the effect of varying time-integrated fluid flux from 5×10^4 mol H_2O/cm^2 (long dashes) to 2×10^5 mol H_2O/cm^2 (short dashes) at a fixed Damköhler number of 5. In the simulations that produced the dotted curves, the time-integrated fluid flux was held constant at 1.1×10^5 mol H_2O/cm^2 and Damköhler number varied from 1.6 (dense dots) to 16 (sparse dots).

[*Burnham et al.*, 1969]. Varying the porosity to as high as 10% had no discernable effect on the geometry of the profile.

[58] Model curves were generated for different values of time-integrated fluid flux and N_D and compared to an isotope data set which derives from 19 whole rock carbonate analyses. Of these, 18 were from the Western Ranges and a single sample, representative of the isotopic composition at the inlet, was located 1 km across strike into the hanging wall of the Purcell Thrust (see Figure 13a). Of 24 carbonate vein analyses, 20 were from the Western Ranges and four were from the hanging wall of the Purcell Thrust (see Figure 13b). Because the difference between vein composition and the composition of immediate wall rocks provides an important constraint on the extent of disequilibrium between rock and fluid, each vein signature was paired with that of an immediate host rock, where relatively undeformed and unaltered protolith was available <0.5 m from the vein. The result is 22 vein-host rock pairs; including 18 from the Western Ranges and four from the Purcell Thrust hanging wall (Figure 13c).

8.2.2. Modeling results and interpretation. [59] The isotope data and model results can be compared on the basis of rock data, fluid composition, and the difference between rock and fluid composition (Figure 13). In this analysis we assume that the composition of vein calcite differs only from that of the fluid by the isotope fractionation factor of 3.8‰ and that the veins are representative of the composition of the latest fluids, an assumption supported by the observation that vein composition does not appear to vary systematically with vein age or type (Figure 6b). The model solution that best fits the data in a least squares sense is represented by the solid curve in Figure 13 and corresponds to a time-integrated fluid flux of 1.1×10^5 mol H_2O cm^{-2} and N_D of 5. Model results for time-integrated fluid fluxes of 5×10^4 mol H_2O cm^{-2} and 2×10^5 mol H_2O cm^{-2} (with N_D constant at 5) are plotted as long dashed curves in Figure 13. Variation in time-integrated fluid flux by a factor of 2 results in a significant degradation in the quality of fit (an increase in sums of squares of more than 300% relative), and our estimates of the time-integrated fluid flux are relatively robust. By comparison, *Ferry* [1992] estimated a time-integrated fluid flux (TIFF) of $\sim 4.0 \times 10^2$ mol H_2O cm^{-2} for a regional hydrothermal cell within low-grade metamorphic rocks of the Appalachians, and various authors have calculated fluxes between 1.2×10^4 and 2.1×10^6 mol H_2O cm^{-2} for ductile fault zones throughout the world [*Dipple and Ferry*, 1992a; *Bowman et al.*, 1994; *Cartwright and Buick*, 1999] (see Table 3). Thus the volume of fluid necessary to cause the observed alteration falls within the range of global values recorded in fault zones but well exceeds that calculated for pervasive flow through low-grade metamorphic terranes. Unless uncharacteristically large quantities of fluid were generated and circulated during greenschist facies metamorphism in the Rockies, water was probably structurally focused into zones with a high density of faults and fractures.

[60] The value of Damköhler number is less well constrained by our analysis. Changes in N_D are manifest in two ways; as N_D is lowered the isotopic front becomes more distended and veins become more depleted relative to their wall rocks. Thus a trade-off exists between accommodating the magnitude of vein-wall rock disequilibrium and obtaining a reasonable match for the shape of the isotopic front. The effect of varying N_D between 1.6 and 16 (at a fixed flux of 1.1×10^5) are illustrated by dotted curves in Figure 13. The degradation in goodness of fit in this instance is not so severe (an increase of 50–100% relative in sums of squares). However, because the model assumptions tend to minimize N_D (as discussed in section 9.5.1), values of N_D lower than 1.6 are not supported by the data. Conversely, measured differences between vein and whole rock carbonate $\delta^{18}O$ greater than 0.2‰ are not consistent with $N_D > 50$ at any time integrated fluid flux greater than $\sim 10^4$ mol cm^{-2} if the samples were distributed along the flow path as indicated in Figure 13. The data therefore constrain N_D to no less than 1.6 and no greater than 50 if our assumed fluid flow trajectory is not in error and if fluid circulation largely predated movement on the Purcell Thrust.

Table 3. Estimated Time-Integrated Fluid Fluxes (TIFF) From Various Terranes

Study	Locality	TIFF, mol H_2O cm^{-2}
Ferry [1992]	Vermont (ankerite metamorphic zone)	4×10^2
Dipple and Ferry [1992a]	Various ductile shear zones	5×10^4 to 2×10^5
Bowman et al. [1994]	Glarus Thrust (mylonite)	$1.2–2.9 \times 10^4$
Cartwright et al. [1999]	Alice Springs Orogen (shear zone)	2.1×10^6
This study	Canadian Rockies (fault and fracture zones)	1.1×10^5

[61] Estimates of N_D may be useful for constraining the efficiency of mineral fluid isotope exchange. Direct comparison of N_D between systems might be of limited value, however, because N_D varies with amount and rate of fluid flow as well as a characteristic distance (L). If, following *Lassey and Blattner* [1988], we adopt for L the length of the aquifer that is infiltrated with externally derived fluids, then the Damköhler number can be expressed as $N_D = kt$, where k is a reaction rate constant and t is the duration of flow. Adopting a timescale of 10^6 years constrains the rate constant for ^{18}O exchange in the Western Ranges to $\sim 10^{-13}$ s^{-1}. This rate constant can be compared to those retrieved from experimental studies. *Cole and Ohmoto* [1986] tabulate exchange rate data for many mineral-fluid systems and distinguish between exchange via surface reaction (e.g., recrystallization) and diffusion. At temperatures of ~370°C, ^{18}O exchange between calcite and H_2O via surface reaction should occur at a rate (r) of $\sim 1.4 \times 10^{-7}$ mol O m^{-2} s^{-1}, where $r = k/a$ and a is the mineral surface area for reaction. The value of k that we extract from the Western Ranges data is reconcilable with this surface reaction rate only at very low values of surface area ($\sim 10^{-2}$ m^{-1}). Because at these temperatures, oxygen isotope exchange via diffusion proceeds at a rate more than 10 orders of magnitude slower than surface reaction [*Cole and Ohmoto*, 1986], an alternate interpretation of the Western Ranges data is that a significant component of oxygen exchange occurred via diffusion. This latter interpretation is consistent with the textures of carbonate rocks in the Western Ranges, which do not present evidence for complete syntectonic recrystallization.

9. Summary and Conclusions

[62] To summarize, data from stable isotopes yield several new insights into the nature of fluid-rock interaction across the hinterland-foreland transition in the Canadian Cordillera:

1. The anomalously low $\delta^{18}O$ of carbonates and tendency of vein compositions to approach average bulk rock $\delta^{18}O$ at individual outcrops in the Dogtooth Range signifies active greater than or equal to meter-scale fluid circulation, but does not require that wall rocks away from fault zones interacted with distally sourced fluids.

2. The Purcell Thrust Fault delineates a 4.7‰ shift toward higher $\delta^{18}O$ values in the Western Ranges. The shift stems from an abrupt change from a siliciclastic to carbonate dominated rock reservoir, but the magnitude of the shift has been diminished due to fluid communication between the Dogtooth and Western Ranges.

3. Wall rocks in the Western Ranges become gradually enriched in $\delta^{18}O$ and approach more typical values for Late Cambrian-Early Ordovician carbonates with increasing distance eastward and upward from the Purcell Thrust.

4. Wall rocks and veins in the Western Ranges are isotopically homogeneous across ≥50 m, indicative of fluid migration across outcrops.

5. Synkinematic veins in the Western Ranges are systematically depleted relative to their immediate host rock, with the largest depletions occurring within cataclasites from regional thrust faults.

6. The pattern of wall rock alteration cannot be explained strictly by variations in age or mineral mode at different outcrops. Likewise, mineral mode and thermal and random (i.e., closed system) kinetic disequilibrium do not justify vein depletions. Instead, deformation-enhanced fluid migration from low-$\delta^{18}O$ siliciclastic rocks in the Dogtooth Range across ≥14 km into the Western Ranges best explains patterns in the composition of veins and wall rocks. During this event, isotopic reaction kinetics were moderately sluggish ($\sim 10^{-13}$ m^{-1}), and time-integrated fluid fluxes were on the order of 10^4–10^5 mol H_2O cm^{-2}. Sluggish exchange of ^{18}O requires either unusually low surface areas available for reaction or a significant component of diffusional exchange. Pervasive pressure solution, stylolitization, and low-displacement faulting provided the enhanced permeability necessary to channel fluids into the Western Ranges, although regional thrust faults also behaved as sites of fluid focusing. In contrast, if fluids migrated across kilometer-scale distances in the Dogtooth Range, they were probably preferentially channeled into regional fault zones.

Appendix A: Stable Isotopic ($\delta^{18}O$) Analysis and Uncertainty

A1. Analytical Techniques

[63] Silicates were crushed and powdered from ~8 cm^3 slabs. For samples that contained both quartz and carbonate, powders were reacted with dilute HCl (10%) and flushed repeatedly with deionized water. All silicates were analyzed at the Queen's University Geochemistry Laboratory (T. K. Kyser, director) using the BrF_5 procedure described by *Clayton and Mayeda* [1963]. A 1σ uncertainty of 0.2‰ was reported for NBS-28, and repeated analyses of blind samples yielded a 1σ of 0.05‰ (N = 4).

[64] Carbonate powders were drilled from slabs using diamond impregnated drill bits in a Dremel© tool. Powders were derived from less than 4 mm^3 of sampled material. Carbonates were analyzed at Queen's (N = 37) and at the UBC Stable Isotope Laboratory (N = 27)(T. F. Pedersen, director). Both laboratories used the techniques outlined by *McCrea* [1950] for liberation of CO_2 by reaction with H_3PO_4. A sample of vein calcite (44-4B) submitted to both laboratories yielded values identical to within 0.1‰. Both laboratories reported an uncertainty (1σ) of <0.1‰ for NBS-19. At Queen's, repeated analyses of blind samples yielded a 1σ of 0.1‰ (N = 4). Similar accuracy was achieved at UBC, where the respective uncertainty for $\delta^{18}O$ was 0.1‰ (N = 5). Values are reported in VSMOW notation and tabulated in Tables A1 and A2.

A2. Reporting of Data and Calculated Uncertainty

[65] Comparisons between data from whole rocks and vein quartz required normalization of the reported value from polyphase silicates with that of quartz. Otherwise, we risk basing erroneous interpretations of disequilibrium between veins and wall rocks on differences in ^{18}O partitioning between coexisting phases. Of 62 silicate analyses, 18 were from polyphase rocks that were too fine grained to permit the use of mineral separation techniques. All but one of these were from the Dogtooth Range. The following methodology was used to equate whole rock silicate values with that of quartz: (1) Mineral modes for each phase were estimated within samples. (2) Using molar volumes presented by *Berman* [1988], mineral mode was converted into the ratio: mol O in phase i versus mol O in 100 cm^3 of sample. (3) A $\delta^{18}O$ equivalent for quartz was calculated by simultaneously solving for mass balance (equation (1)) and isotopic fractionation between phase i and quartz (equation (2)):

$$\delta^{18}O_{wr} = \sum_{i=1} X_{O,i}\delta^{18}O_i \quad \text{(A1)}$$

$$\delta^{18}O_{quartz} - \delta^{18}O_i = \Delta_{quartz-I} \quad \text{(A2)}$$

where $\delta^{18}O_{wr}$ is the reported oxygen isotope composition of the whole rock sample; $X_{O,i}$ represents the molar fraction of oxygen contained within phase i over that within 100 cm^3 of sample; and $\Delta_{quartz-i}$ is the fractionation factor between phase i and quartz (as from *Rumble* [1982]).

[66] Fractionation factors for the systems quartz-muscovite, quartz-clinochlore, and quartz-albite were taken from *Zheng* [1993a, 1993b], *Clayton et al.* [1972], and *O'Neil and Taylor* [1969]. On the basis of the results of calcite-dolomite solvus

Table A1. Stable Isotope Data From the Western Ranges[a]

Locality	Sample	Mineral	Description	Rock Composition, vol %				$\delta^{18}O$	$\delta^{18}O$(Qtz)	$d^{13}C$
				Qtz	Musc	Chl	Plag/Ksp	(Measured)	370°C	(PDB)
Purcell Thrust Fault (9)	11-1B-WR	silicate	siliceous slate	60	40	0	0	14.7	16.3	
				45	55	0	0		17	
	10-5C-WR	silicate	slate (50 cm from hanging wall splay)	60	40	0	0	13.8	15.4	
				0	100	0	0		18	
				35	35	30	0		16.8	
	10-5C-VQ	quartz	fault-parallel vein					18.1		
	10-5A-VQ	quartz	fault-parallel, crack-seal vein					18.3		
	10-5A-VC	calcite	fault-parallel, crack-seal vein					16.2		−1.9
	34-4A-WR	calcite	calcareous siltstone					16.0		−1.9
	34-4A-VC	calcite	sigmoidal tension gash					16.0		−2.2
	11-4C-VC	calcite	en echelon tension gash					16.2		−2.7
	35-1A-VC	calcite	en echelon tension gash					16.3		−2.5
hw	34-5C-WR	silicate	phyllite	0	100	0	0	15.6	19.8	
fw	34-5A-VQ	quartz	fault-parallel, laminated vein					18.0		
	34-5A-VC	calcite	fault-parallel, laminated vein					16.2		−2.7
	34-5B-VQ	silicate	fault-parallel, laminated vein (1 m away along strike)					18.7		
	34-5B-VC	calcite	fault-parallel, laminated vein					16.2		−2.7
	34-6B-WR	calcite	calcareous slate					17.9		−2.4
	12-2C-VC	calcite	bedding-parallel/ laminated vein					16.5		−0.6
	35-3B-VQ	quartz	fault-parallel vein (footwall splay)					19.0		
	35-3B-VC	calcite	fault-parallel vein (footwall splay)					16.5		−0.4
	12-3C-WR	silicate	siliceous slate	60	30	10	0	15.7	17.4	
				70	30	0	0		16.9	
McKay-Canyon Creek Contact at Rocky Mountain Trench (10)	41-1B-WR	calcite	limestone					19.0		0.3
	41-1C-WR	calcite	calcareous siltstone					19.2		−0.1
	41-1C-VC	calcite	crosscutting/folded vein					18.9		−0.2
	41-1D-WR	calcite	slate					18.8		−0.1
	41-2A-VC	calcite	fault-parallel vein					19.1		−0.3
McKay Group	41-2A-WR	calcite	sparry limestone					19.1		0.3
Canyon Creek Formation	41-3B-WR	calcite	calcareous slate					18.1		0.3
McKay Group at Mitchell Road	96MRA4	calcite	micrite					18.5		−1.2
Rocky Mountain Trench (11)	96MRA4	quartz	crosscutting/folded vein					20.6		
	96MRA4	calcite	crosscutting/folded vein					18.1		−1.1
	96MRB1	calcite	micrite					18.0		0.7
	96MRB4	calcite	micrite					18.3		−1.2
	96MRB7	calcite	crack-seal, cleavage-parallel/orthogonal vein					18.2		−1.0
	96MRB7	quartz	crack-seal, cleavage-parallel/orthogonal vein					20.5		
	96MRB5	calcite	boudinaged, cleavage-parallel vein					18.1		7−1.2
	96MRB6	calcite	boudinaged, cleavage-parallel vein					18.1		7−1.2
	96MRC3	calcite	micrite					18.6		−1.2
	96MRC3N	calcite	bleached nodule					17.8		−0.3

Table A1. (continued)

Locality	Sample	Mineral	Description	Rock Composition, vol %				$\delta^{18}O$ (Measured)	$\delta^{18}O$(Qtz) 370°C	$d^{13}C$ (PDB)
				Qtz	Musc	Chl	Plag/Ksp			
	96MRC5	calcite	cleavage-parallel vein					17.9		−1.5
	96MRC6	calcite	fault-parallel vein					18.0		−1.5
	96MRC8	calcite	cleavage-parallel vein					18.0		−1.6
	96MRD4	calcite	micrite					18.5		−1.8
	96MRD1	calcite	fault-parallel vein					18.0		−1.1
	96MRD2	calcite	fault-parallel vein					18.3		−1.4
	96MRD7	calcite	tensile cracks (mode I)					18.1		−1.1
McKay Group (Unit 4)	41-4A-VQ	quartz	tensile cracks (mode I)					22.3		
4.5 km east of Golden at Trans-Canada Highway (unnumbered)	41-4A-VC	calcite	tensile cracks (mode I)					20.0		−0.3
	41-4A-WR	calcite	limestone					20.1		−0.2
	41-4B-WR	calcite	calcareous slate					20.4		−0.3
Unnamed fault, Beaverfoot Formation at Mount Moberly (12A)	49-2A-WRV	dolomite	vein (breccia)					21.8		−2.6
	49-2A-WRV	calcite	vein (breccia)					23.1		−2.7
	49-2A-WRM	dolomite	matrix (breccia)					22.4		−0.9
	49-2A-WRM	calcite	matrix (breccia)					23.1		−1.0
	49-1A-WR	dolomite	dolostone (protolith)					22.9		−0.7
Unnamed fault, Beaverfoot Formation at Trans-Canada Highway (12B)	36-1B-WRV	calcite	vein (breccia)					22.5		−1.3
	36-1B-WRV	dolomite	vein (breccia)					22.3		−1.1
	36-1B-WRM	calcite	matrix (breccia)					25.1		−0.6
	36-1B-WRM	dolomite	matrix (breccia)					24.1		−0.4
	36-1A-WR	calcite	dolostone (hw)					23.8		−1.5
	36-1B-WR	calcite	lime/dolostone (fw-protolith)					26.2		−0.7
Unnamed fault, McKay Group (13)	29-1H-WR	calcite	limestone (5 m from fault)					20.8		−1.5
hw	29-1A-WR	calcite	limestone (30 cm from fault)					20.8		−1.7
	29-1D-WR	calcite	matrix (breccia)					20.0		−1.6
	29-1D-VC	calcite	vein (breccia)					19.8		−1.3
fw	29-1G-WR	calcite	limestone (1 m from fault)					20.9		−1.4
	29-1F-WR	calcite	limestone (3 m from fault)					20.7		−1.7

[a] Qtz, quartz; Musc, muscovite; Chl, chlorite; Plag/Ksp, plagioclase/potassium feldspar; hw, hanging wall; fw, footwall.

thermometry of *Kubli* [1990] and *Gardner* [1977] and isotope thermometry in this study (discussed below), we assigned a temperature of 370°C for isotopic equilibration across the transect. The above technique involves uncertainty in the estimation of mineral mode, the temperature of equilibration, and the selection of fractionation factors. We used the following strategy to account for each of these:

1. In most cases, quartz, albite, muscovite, and chlorite were easily distinguished through a polarizing microscope, thereby enabling easy visual estimation of mineral mode. Thin sections were cut perpendicular to foliation to avoid overestimation of the concentration of sheet silicates. In very fine grained slates, X-ray diffraction spectrometry confirmed relative abundances of chlorite and muscovite. Depending on the grain size and textural complexity within samples, an uncertainty of 5–20% was assigned to each estimation of mineral mode.

2. Because peak conditions never exceeded chlorite grade metamorphism, 400°C represents a conservative maximum for temperatures in the study area. In the Dogtooth Range the shallowest units reached a burial depth of at least 10 km [*Kubli*, 1990], which, assuming a geothermal gradient of +30°C km^{-1}, is consistent with a minimum temperature of 300°C. We therefore varied temperatures between 300°C and 400°C in our sensitivity analysis.

3. Finally, fractionation factors from *Zheng* [1993a, 1993b] were replaced with those of *Clayton and Keiffer* [1991] (quartz-albite), *Wenner and Taylor* [1971] (quartz-chlorite), and *Chacko et al.* [1996] (quartz-muscovite) and substituted into the $\Delta_{quartz-i}$ term of (A2). The predicted uncertainties, which arise from changing one of conditions 1–3 while holding the other two constant, are presented in Table A3. Under these assumptions the uncertainty exceeded ±0.5‰ and ±1.0‰ only in samples 6 and 2, respectively. Of those, the highest error was ±2.1‰ (sample 13-1A).

Table A2. Stable Isotope Data From the Dogtooth Range

Locality	Sample	Mineral	Description	Rock Composition, vol %				$\delta^{18}O$	$\delta^{18}O$ (Qtz)	$d^{13}C$
				Qtz	Musc	Chl	Plag/Ksp	(Measured)	370°C	(PDB)
Copperstain Syncline (unnumbered)	42-1A-WR	calcite	limestone					15.4		1.5
	42-4C-WR	calcite	calcareous siltstone					15.8		0.09
	42-4B-VQ	quartz	type I, sigmoidal vein					18.9	18.9	
	42-4A-VC	calcite	type I, sigmoidal vein					16.0		3.0
	42-4A-VQ	quartz	type I, sigmoidal vein					19.7		
	42-5B-WR	silicate	phyllite	20	80	0	0	16.5	19.9	
				10	90	0	0		20.2	
	42-5C-VQ	quartz	type II, cleavage-parallel vein					18.2		
	42-5C-VH2	muscovite	phyllite							
	42-5C-VH	chlorite	type II, cleavage-parallel vein							
Heather Mountain Thrust at Quartz Creek (2)	17-3C-WR	silicate	calcareous slate	5	60	35	0	10.8	15.1	
				5	55	40	0		15.1	
	17-3C-WR	calcite	calcareous slate					15.7		−2.8
	17-3D-WR	silicate	phyllite	0	80	20	0	13.7	18.1	
				0	60	40	0		18.3	
	17-3E-VQ	quartz	type I, antitaxial vein					15.7		
	17-3E-VC	calcite	type I, antitaxial vein					13.8		−2.4
	17-3E-WR	dolomite	dolostone					17.3		−0.9
	17-3F-WR	silicate	sandstone	90	0	0	10	13.6	13.8	
				95	0	0	5		13.7	
hw	17-3F-VQ	quartz	quartz veinlet					13.9		
fw	17-3G-WR	silicate	chlorite phyllite	0	70	30	0	9.5	14	
				0	95	5	0		13.7	
	17-3H-WR	chlorite	chlorite phyllite	0	0	100	0	9.3	14.5	
	17-3K-WR	silicate	chlorite phyllite	20	5	75	0	10.2	14.2	
				40	5	55	0		13.2	
Heather Mountain Thrust at Heather Mountain (1)	16-2B-WR	silicate	sandstone	95	5	0	0	13.4	13.6	
				100	0	0	0		13.4	
	16-2D-WR	silicate	phyllite	5	55	40	0	10.0	14.3	
				25	55	30	0		13.4	
fw	16-2E-WR	silicate	quartzite	85	0	0	15	12.5	12.8	
				95	0	0	5		12.6	
	16-2G-WR	silicate	quartzite	40	55	0	5	11.1	13.5	
				60	35	0	5		12.6	
	16-2I-WR	silicate	quartzite	80	15	0	5	11.9	12.6	
				90	10	0	0		12.3	
	16-2I-VQ	quartz	type I, antitaxial vein		13.1					
	16-3B-VC	calcite	type I, antitaxial vein					16.3		−0.4
	16-3B-VH	muscovite	type I, antitaxial vein							
Prairie Hills Thrust-hw	16-3B-WR	dolomite	dolostone					15.5		1.6
	16-1A-WR	silicate	quartzite	85	15	0	0	12.3	12.9	
fw				95	5	0	0		12.5	
Quartz Creek Thrust at Dauntless Ridge (4)	43-4A-WR	silicate	type III vein, shear zone	90	10	0	0	13.1	13.5	
				80	20	0	0		13.9	
	43-4B-WR	quartz	quartzite					12.5		
Quartz Creek Thrust at Kinbasket Lake (3)	34-1C-WR	silicate	phyllite	15	85	0	0	12.2	15.7	
				5	95	0	0		16.2	
	34-2B-VQ	quartz	type III, cleavage/fault-parallel vein					14.7		
hw	34-2B-VC	calcite	type III, cleavage/fault-parallel vein					14.1		−11.6

Table A2. (continued)

Locality	Sample	Mineral	Description	Rock Composition, vol % Qtz	Musc	Chl	Plag/Ksp	$\delta^{18}O$ (Measured)	$\delta^{18}O$ (Qtz) 370°C	$d^{13}C$ (PDB)
fw	34-2A-WR	silicate	foliated quartzite	80	15	0	5	14.2	15	
				90	5	0	5		14.5	
	34-2A-WR	calcite	foliated quartzite					14.7		−9.9
	34-3B-VQ	quartz	type II, cleavage-parallel vein					14.5		
	34-3C-VQ	quartz	type II, cleavage-parallel vein					14.5		
Unnamed fault(footwall of Wall Creek Thrust) (6)	18-2G-WR	silicate	quartzite	95	5	0	0	12.9	13.1	
				85	15	0	0		13.5	
	18-2E-WR	silicate	quartzite	95	5	0	0	12.7	12.9	
				90	10	0	0		13.1	
	18-2E-VQ	quartz	type I, fibrous vein					18.8		
	18-2A-WR	silicate	quartzite	90	5	0	5	12.3	12.5	
				85	10	0	5		12.7	
	18-3B-VQ	quartz	type II, cleavage-parallel vein					13.4		
	18-3B-WR	silicate	slate	0	90	10	0	10.5	14.7	
hw				0	95	5	0		14.7	
fw	18-3C-VQ	quartz	type I, fibrous, a-c vein					12.9		
	18-3C-WR	silicate	foliated quartzite	65	30	0	5	11.8	13.2	
				80	15	0	5		12.5	
	18-3D-VN	chlorite/quartz	matrix within foliated vein	90	0	10	0	11.7	12.2	
				70	5	25	0		13.2	
	18-3D-VQ	quartz	type II, deformed, crack-seal vein					12.5		
	18-3E-WR	silicate	foliated quartzite	90	10	0	0	11.1	11.5	
				80	20	0	0		11.9	
	18-3E-VQ	quartz	type I, fibrous vein					12.7		
Cirque Creek Thrust (8)	23-3C-VQ	quartz	type III, 3-m-wide vein					13.1		
Wiseman Creek Thrust at Kinbasket Lake (5)	14-3A-WR	silicate	foliated grit	90	8	0	2	14.9	15.3	
				95	3	0	2		15.1	
	14-2A-VQ	quartz	vein/quartzite-fault zone					14.9		
	14-4C-WR	silicate	foliated sandstone	60	35	5	0	12.8	14.5	
				50	45	5	0		14.9	
	14-4A-WR	silicate	foliated sandstone	75	25	0	0	13.8	14.8	
				60	40	0	0		15.4	
	14-1F-WR	silicate	foliated sandstone	60	40	0	0	11.9	13.5	
				40	60	0	0		14.4	
Wiseman Creek Thrust at Oldman Creek (7)	9-2E-WR	silicate	sandstone	95	5	0	0	13.2	13.4	
				85	15	0	0		13.8	
	9-1D-WR	calcite	limestone					15.3		4.2
	13-1A-WR	silicate	calcareous slate	33	33	33	0	15.1	18.2	
				50	50	0	0		17.1	
hw				0	100	0	0		19.3	
fw	13-4A-VQ	quartz	massive quartz vein at fault					14.1		
	13-4B-WR	quartz	quartzite matrix	100	0	0	0	13.9	13.9	
				95	5	0	0		14.1	
	13-4B-VQ	quartz	massive quartz vein/7m from fault					13.1		
	13-4C-WR	silicate	quartzite matrix	85	15	0	0	12.2	12.8	
				95	5	0	0		12.4	
	8-2-WR	quartz	quartzite protolith	100	0	0	0	13.2	13.2	
				95	3	0	2		13.4	
	48-5A-WR	quartz	quartzite					14.7		

Table A3. Predicted Uncertainties (±1σ) in Conversion of Whole Rock $\delta^{18}O$ to Quartz Equivalent Values

Sample	Mineral Mode, ±‰	Temperature, ±‰	Fractionation Factor, ±‰
42-5B	0.15	0.4	0.3
17-3C	< 0.05	0.55	0.05
17-3G	0.15	0.6	0.05
17-3K	0.5	0.5	0.65
16-2D	0.45	0.55	0.15
16-2G	0.45	0.3	0.25
43-4A	0.2	0.05	<0.1
34-1C	0.25	0.45	0.35
34-2A	0.25	0.1	<0.1
18-3B	<0.05	0.5	0.25
18-3C	0.35	0.15	0.15
14-4C	0.2	0.2	0.1
14-4A	0.3	0.15	0.1
14-1F	0.45	0.2	0.15
13-1A	2.1	0.35	0.15
10-5C	1.3	0.2	0.15
34-5C	0.5	0.5	0.4
12-3C	0.25	0.3	<0.05

[67] **Acknowledgments.** The authors are indebted to Phil Simony, who was indispensable in highlighting the salient aspects of the eastern Cordillera. We thank Kurt Kyser and Kerry Klassen at Queen's and Bente Nielsen at UBC for their responsiveness to questions regarding isotopic analyses. Keith Lassey kindly and promptly provided copies of FORTRAN routines that were essential for the reactive transport modeling. Chris Akelaitis and Jennifer Dicus were ambitious and insightful field assistants. This project was supported in part by NSERC operating grants to Lori Kennedy and Greg Dipple. A GSA student research grant and a Thomas and Marguerite McKay scholarship also provided funding to Stuart Knoop. Reviews by Nick Oliver and David Gray led to improvements in the clarity of the manuscript.

References

Anovitz, L. M., and E. J. Essene, Phase equilibria in the system $CaCO_3$-$MgCO_3$-$FeCO_3$, *J. Petrol.*, *28*, 389–414, 1987.

Balkwill, H. R., Structural analysis of the Western Ranges, Rocky Mountains, near Golden, British Columbia, Ph.D thesis, Univ. of Tex. at Austin, Austin, 1969.

Balkwill, H. R., Structural geology, Lower Kicking Horse River region, Rocky Mountains, British Columbia, *Bull. Can. Pet. Geol.*, *20*, 608–633, 1972.

Berman, R. G., Internally-consistent thermodynamic data for minerals in the system Na_2O-K_2O-CaO-MgO-FeO-Fe_2O_3-Al_2O_3-SiO_2-TiO_2-H_2O-CO_2, *J. Petrol.*, *29*, 2445–2552, 1988.

Bickle, M. J., Transport mechanisms by fluid-flow in metamorphic rocks; oxygen and strontium decoupling in the Trois Seigneurs Massif: A consequence of kinetic dispersion?, *Am. J. Sci.*, *292*, 289–316, 1992.

Bickle, M. J., and D. McKenzie, The transport of heat and matter by fluids during metamorphism, *Contrib. Mineral. Petrol.*, *95*, 384–392, 1987.

Bickle, M. J., and D. McKenzie, Transport mechanisms by fluid-flow in metamorphic rocks: Oxygen and strontium decoupling in the Trois Seigneurs Massif: A consequence of kinetic dispersion?, *Am. J. Sci.*, *292*, 289–316, 1992.

Bowman, J. R., S. D. Willett, and S. J. Cook, Oxygen isotopic transport and exchange during fluid flow: One-dimensional models and applications, *Am. J. Sci.*, *294*, 1–55, 1994.

Bradbury, H. J., and G. R. Woodwell, Ancient fluid flow within foreland terrains, in *Fluid Flow in Sedimentary Basins and Aquifers*, edited by J. C. Goff and B. P. J. Williams, *Geol. Soc. Spec. Publ.*, *34*, 87–102, 1987.

Brady, J. B., The role of volatiles in the thermal history of metamorphic terranes, *J. Petrol.*, *29*, 1187–1213, 1988.

Burkhard, M., and R. Kerrich, Fluid regimes in the deformation of the Helvetic nappes, Switzerland, as inferred from stable isotope data, *Contrib. Mineral. Petrol.*, *99*, 416–429, 1988.

Burnham, C. W., J. R. Holloway, and N. F. Davis, Thermodynamic properties of water to 1000°C and 10,000 bars, *Spec. Pap. Geol. Soc. Am.*, *132*, 1969.

Cartwright, I., and I. S. Buick, The flow of surface-derived fluids through Alice Springs age middle-crustal ductile shear zones, Reynolds Range, central Australia, *J. Metamorph. Geol.*, *17*, 397–414, 1999.

Cartwright, I., W. L. Power, N. H. S. Oliver, R. K. Valenta, and G. S. Mclatchie, Fluid migration and vein formation during deformation and greenschist facies metamorphism at Ormiston Gorge, central Australia, *J. Metamorph. Geol.*, *12*, 373–386, 1994.

Chacko, T., X. Hu, T. K. Mayeda, R. N. Clayton, and J. R. Goldsmith, Oxygen isotope fractionations in muscovite, phlogopite, and rutile, *Geochimica et Cosmochimica Acta*, *60*, 2597–2608, 1996.

Clayton, R. N., and S. W. Keiffer, Oxygen isotopic thermometer calibrations, in *Stable Isotope Geochemistry: A Tribute to Samuel Epstein*, edited by H. P. Taylor, J. R. O'Neil, and I. R. Kaplan, *Spec. Publ. Geochem. Soc.*, *3*, 3–10, 1991.

Clayton, R. N., and T. K. Mayeda, The use of bromine pentafluoride in the extraction of oxygen from oxides and silicates for isotopic analysis, *Geochim. Cosmochim. Acta*, *27*, 43–52, 1963.

Clayton, R. N., J. R. O'Neil, and T. K. Mayeda, Oxygen isotope exchange between quartz and water, *J. Geophys. Res.*, *77*, 3057–3067, 1972.

Cole, D. R., and H. Ohmoto, Kinetics of isotopic exchange at elevated temperatures and pressures, in *Stable Isotopes in High Temperature Geological Processes*, *Rev. Mineral*, vol. 16, edited by J. W. Valley, H. P. Taylor, and J. R. O'Neil, pp. 41–90, Mineral. Soc. of Am., Washington, D. C., 1986.

Cook, D. G., Structural style influenced by lithofacies, Rocky Mountain Main Ranges, Alberta British Columbia, *Bull. Geol. Surv. Can.*, *233*, 1975.

Cox, S. F., and M. A. Etheridge, Coupled grain-scale dilatancy and mass transfer during deformation at high fluid pressures: Examples from Mount Lyell, Tasmania, *J. Struct. Geol.*, *11*, 147–162, 1989.

Dipple, G. M., Reactive dispersion of stable isotopes by mineral reaction during metamorphism, *Geochim. Cosmochim. Acta*, *62*, 3745–3752, 1998.

Dipple, G. M., and J. M. Ferry, Metasomatism and fluid flow in ductile fault zones, *Contrib. Mineral. Petrol.*, *112*, 149–164, 1992a.

Dipple, G. M., and J. M. Ferry, Fluid flow and stable isotopic alteration in rocks at elevated temperatures with applications to metamorphism, *Geochim. Cosmochim. Acta*, *56*, 3539–3550, 1992b.

Etheridge, M. A., V. J. Wall, S. F. Cox, and R. H. Vernon, High fluid pressures during regional metamorphism and deformation: Implications for mass transport and deformation mechanisms, *J. Geophys. Res.*, *89*, 4344–4358, 1984.

Ferry, J. M., Regional metamorphism of the Waits River Formation, eastern Vermont: Delineation of a new type of giant metamorphic hydrothermal system, *J. Petrol.*, *33*, 45–94, 1992.

Fisher, D. M., and S. L. Brantley, Models of quartz overgrowth and vein formation: Deformation and episodic fluid flow in an ancient subduction zone, *J. Geophys. Res.*, *97*, 20,043–20,061, 1992.

Gabrielse, H., and C. J. Yorath, Introduction, in *Geology of the Cordilleran Orogen in Canada*, *Geol. Can.*, vol. 4, edited by H. Gabrielse and C. J. Yorath, pp. 3–11, Geol. Surv. of Can., Ottawa, 1992.

Gardner, D. A. C., Structural geology and metamorphism of calcareous lower Paleozoic slates, Blaeberry River-Reburn Creek area, near Golden, British Columbia, Ph.D. thesis, Queen's Univ., Kingston, Ont., Canada, 1977.

Gardner, D. A. C., R. A. Price, and D. M. Carmichael, The petrology and structural fabric of some Paleozoic calcareous pelites in the Porcupine Creek Anticlinorium near Golden, British Columbia, *Pap. Geol. Surv. Can.*, *76-1A*, 137–140, 1976.

Ghent, E. D., and J. R. O'Neil, Late Precambrian marbles of unusual carbon-isotope composition, southeastern British Columbia, *Can. J. Earth Sci.*, *22*, 324–329, 1985.

Gray, D. R., R. T. Gregory, and D. W. Durney, Rock-buffered fluid-rock interaction in quartz rich turbidite sequences, eastern Australia, *J. Geophys. Res.*, *96*, 19,681–19,704, 1991.

Kirschner, D. L., and L. A. Kennedy, Limited syntectonic fluid flow in carbonate-hosted thrust faults of the Front Ranges, Canadian Rockies, inferred from stable isotope data and structures, *J. Geophys. Res.*, *106*, 8827–8840, 2001.

Knoop, S. R., A stable isotopic analysis of syn-tectonic fluid regimes in the Dogtooth, Western, and Main Ranges of southeastern British Columbia, M.Sc. thesis, Univ. of B. C., Vancouver, Canada, 2000.

Kubli, T. E., Geology of the Dogtooth Range, northern Purcell Mountains, British Columbia, Ph.D. thesis, Univ. of Calgary, Calgary, Alberta, Canada, 1990.

Kubli, T. E., and P. S. Simony, The Dogtooth High, northern Purcell Mountains, British Columbia, *Bull. Can. Pet. Geol.*, *40*, 36–51, 1992.

Kubli, T., and P. S. Simony, The Dogtooth Duplex, a model for the structural development of the northern Purcell Mountains, *Can. J. Earth Sci.*, *31*, 1672–1686, 1994.

Lassey, K. R., On the computation of certain integrals containing the modified Bessel function I_0 (ξ), *Math. Comput.*, *39*, 625–637, 1982.

Lassey, K. R., and P. Blattner, Kinetically controlled oxygen isotope exchange between fluid and rock in one-dimensional advective flow, *Geochim. Cosmochim. Acta*, *52*, 2169–2175, 1988.

Lee, Y.-J., D. L. Wiltschko, E. L. Grossman, J. W. Morse, and W. M. Lamb, Sequential vein growth with fault displacement: An example from the Austin Chalk Formation, Texas, *J. Geophys. Res.*, *102*, 22,611–22,628, 1997.

Logan, J. M., The influence of fluid flow on the mechanical behavior of faults, *Proc. Symp. Rock Mech.*, *33rd*, 141–149, 1992.

Machel, H. G., P. A. Cavell, and K. S. Patey, Isotopic evidence for carbonate cementation and recrystallization, and for tectonic expulsion of fluids into the Western Canada Sedimentary Basin, *Geol. Soc. Am. Bull.*, *108*, 1108–1119, 1996.

Marquer, D., and M. Burkhard, Fluid circulation, progressive deformation and mass-transfer processes in the upper crust: The example of basement-cover relationships in the external crystalline massifs, Switzerland, *J. Struct. Geol.*, *14*, 1047–1057, 1992.

McCaig, A. W., Deep fluid circulation in fault zones, *Geology*, *16*, 867–870, 1988.

McCrea, J. M., On the isotope chemistry of carbonates and a paleotemperature scale, *J. Chem. Phys.*, *18*, 849–857, 1950.

Nesbitt, B. E., and K. Muehlenbachs, Paleohydrology of the Canadian Rockies and origins of brines, Pb-Zn deposits and dolomitization in the Western Canada Sedimentary Basin, *Geology*, *22*, 243–246, 1994.

Nesbitt, B. E., and K. Muehlenbachs, Geochemistry of syn-tectonic, crustal fluid regimes along the Lithoprobe Southern Canadian Cordillera Transect, *Can. J. Earth Sci.*, *32*, 1699–1719, 1995.

Nesbitt, B. E., and K. Muehlenbachs, Paleo-hydrology of late Proterozoic units of southeastern Canadian Cordillera, *Am. J. Sci.*, *297*, 359–392, 1997.

Oliver, J., Fluids expelled tectonically from orogenic belts: Their role in hydrocarbon migration and other geologic phenomena, *Geology*, *14*, 99–102, 1986.

Oliver, N. H. S., Review and classification of structural controls on fluid flow during regional metamorphism, *J. Metamorph. Petrol.*, *14*, 477–492, 1996.

O'Neil, J. R., and H. P. Taylor Jr., Oxygen isotope equilibrium between muscovite and water, *J. Geophys. Res.*, *74*, 6012–6022, 1969.

O'Neil, J. R., R. N. Clayton, and T. K. Mayeda, Oxygen isotope fractionation in divalent metal carbonates, *J. Chem. Phys.*, *51*, 5547–5558, 1969.

Price, R. A., and P. Simony, Geology of the Lake Louise–Golden area, map, Alberta Soc. of Pet. Geol., Calgary, 1971.

Rumble, D., Stable isotope fractionation during metamorphic devolatilization reactions, in *Characterization of Metamorphism Through Mineral Equilibria*, *Rev. Mineral.*, vol. 10, edited by J. M. Ferry, pp. 327–353, Mineral. Soc. of Am., Washington, D. C., 1982.

Rye, D. M., and H. J. Bradbury, Fluid flow in the crust: An example from a Pyrenean thrust ramp, *Am. J. Sci.*, *288*, 197–235, 1988.

Sharp, Z. D., and D. L. Kirschner, Quartz-calcite oxygen isotope thermometry: A calibration based on natural isotopic variations, *Geochim. Cosmochim. Acta*, *58*, 4491–4501, 1994.

Sibson, R. H., Structural permeability of fluid-driven fault-fracture meshes, *J. Struct. Geol.*, *18*, 1031–1042, 1996.

Simony, P. S., and G. Wind, Structure of the Dogtooth Range and adjacent portions of the Rocky Mountain Trench, in *Structure of the Southern Canadian Cordillera*, edited by J. O. Wheeler, *Spec. Pap. Geol. Assoc. Can.*, *6*, 41–51, 1970.

Valley, J., Stable isotope geochemistry of metamorphic rocks, in *Stable Isotopes in High Temperature Geological Processes*, *Rev. Mineral.*, vol. 16, edited by J. W. Valley, H. P. Taylor, and J. R. O'Neil, pp. 445–489, Mineral. Soc. of Am., Washington, D. C., 1986.

van der Velden, A. J., and F. A. Cook, Structure and tectonic development of the southern Rocky Mountain Trench, *Tectonics*, *15*, 517–544, 1996.

Veizer, J., Trace elements and isotopes in sedimentary carbonates, in *Carbonates: Mineralogy and Chemistry, Rev. Mineral.*, vol. 11, edited by R. J. Reeder, pp. 265–299, Mineral. Soc. of Am., Washington, D. C., 1983.

Veizier, J., and J. Hoefs, The nature of O^{18}/O^{16} and C^{13}/C^{12} secular trends in sedimentary carbonate rocks, *Geochim. Cosmochim. Acta*, *40*, 1387–1395, 1976.

Wenner, D. B., and H. P. Taylor Jr., Temperatures of serpentinization of ultramafic rocks based on O^{18}/O^{16} fractionation between coexisting serpentine and magnetite, *Contrib. Mineral. Petrol.*, *32*, 165–185, 1971.

Woodwell, G. R., Fluid Migration in an overthrust sequence of the Canadian Cordillera, Ph.D. thesis, Yale Univ., New Haven, Conn., 1985.

Yao, Q., and R. V. Demicco, Paleoflow patterns of dolomitizing fluids and paleohydrogeology of thesouthern Canandian Rocky Mountains: Evidence from dolomite geometry and numerical modeling, *Geology*, *23*, 791–794, 1995.

Yao, Q., and R. V. Demicco, Dolomitization of the Cambrian carbonate platform, southern Canadian Rocky Mountains: Dolomite front geometry, fluid inclusion geochemistry, isotopic signature, and hydrogeologic modeling studies, *Am. J. Sci.*, *297*, 892–938, 1997.

Zheng, Y.-F., Calculation of oxygen isotope fractionation in anhydrous silicate minerals, *Geochim. Cosmochim. Acta*, *57*, 1079–1091, 1993a.

Zheng, Y.-F., Calculation of oxygen isotope fractionation in hydroxyl-bearing silicates, *Earth Planet. Sci. Lett.*, *120*, 247–263, 1993b.

Zheng, Y.-F., Oxygen isotope fractionation in carbonate and sulfate minerals, *Geochem. J.*, *32*, 109–126, 1999.

G. M. Dipple, L. A. Kennedy, and S. R. Knoop, Department of Earth and Ocean Science, University of British Columbia, 6339 Stores Rd., Vancouver, British Columbia, Canada V6T 1Z4. (dipple@eos.ubc.ca; lkennedy@eos.ubc.ca; sknoop@loadmail.com)